DETERMINING PRESSURE LOSSES FOR AIRFLOW IN RESIDENTIAL DUCTWORK

A Thesis

by

KEVIN DOUGLAS WEAVER

Submitted to the Office of Graduate Studies of
Texas A&M University
in partial fulfillment of the requirements for the degree of

MASTER OF SCIENCE

December 2011

Major Subject: Mechanical Engineering

DETERMINING PRESSURE LOSSES FOR AIRFLOW IN RESIDENTIAL DUCTWORK

A Thesis

by

KEVIN DOUGLAS WEAVER

Submitted to the Office of Graduate Studies of
Texas A&M University
in partial fulfillment of the requirements for the degree of

MASTER OF SCIENCE

Approved by:

Chair of Committee,	Charles Culp
Committee Members,	David Claridge
	Jeff Haberl
Head of Department,	Jerald A. Caton

December 2011

Major Subject: Mechanical Engineering

ABSTRACT

Determining Pressure Losses for Airflow

in Residential Ductwork. (December 2011)

Kevin Douglas Weaver, B.S., Texas A&M University

Chair of Advisory Committee: Dr. Charles H. Culp

Airflow pressure losses through rigid metallic and non-metallic flexible ducts were studied and recommendations to improve the rating of flexible ducts were made as part of this study. The testing was done in compliance with ASHRAE Standard 120-1999, Methods of Testing to Determine Flow Resistance of HVAC Air Ducts and Fittings (*ASHRAE 1999*). Duct sizes of 6", 8", and 10" were tested in a positive pressure, blow-through configuration. An As-Built Test Protocol expands the test configurations specified by Standard 120-1999. Results of the current tests extend the existing ASHRAE/ACCA data for flexible duct which does not include pressure loss data for flexible ducts that are compressed beyond approximately 4%. The data from this study exhibit higher pressure drops than prior ACCA or ASHRAE data. Some configurations exhibit over ten times the pressure loss found in rigid duct or fully stretched flexible duct of the same diameter.

ACKNOWLEDGEMENTS

This study could not have occurred without the guidance and direction of my advisor, Dr. Charles Culp. I also appreciate the guidance of my advisory committee, Dr. David Claridge and Dr. Jeff Haberl. Credit is also due to Mr. Michael Chadwell for assistance in programming, to Mr. Blake Clements for assistance in data collection, and to Mr. David Cantrill for assistance in documentation of operating code.

This study was funded by the Air Distribution Institute, American Society of Heating, Refrigerating, and Air-Conditioning Engineers (ASHRAE), Oncor Electric Delivery and Lennox Industries. I sincerely thank them for their support of this research.

TABLE OF CONTENTS

LIST OF FIGURES

LIST OF TABLES

CHAPTER I

INTRODUCTION

Static pressure losses through residential duct systems affect residential heating, ventilation, and air conditioning (HVAC) equipment energy efficiency and performance. Energy consumption impacts end users, ranging from large commercial structures to homeowners. Residential heating and cooling systems consume on-average approximately 29% of the residential energy consumption (Department of Energy 2005)[1]. This has resulted in an effort for more efficient home systems.

Home HVAC unit efficiency has improved as demonstrated by higher Seasonal Energy Efficiency Ratio (SEER) systems that are now available on the market and the historical increase in SEER requirement. A minimum SEER value of 10 took effect in 1992 (DOE 1992)[2]. In January of 2006, the requirement increased to 13 SEER (DOE 2005)[1]. However, cooling equipment improvements represent only a partial solution to the efficiency problem. The efficiency of the duct system, delivery performance, and associated installation can have an effect on the overall efficiency of a heating and cooling system, and thus must be evaluated and improved as well.

Duct systems are typically designed based on required cooling capacity. As explained in Air Conditioning Contractors of America (ACCA) Manual D (ACCA 1995)[3], the contractor first decides how much air each space requires, usually based on the maximum assumed cooling load and an assumed temperature difference. The

---

This thesis follows the style and format of the *ASHRAE Journal.*

corresponding duct size to that space is then chosen based on the volumetric flow capacity requirements for the selected duct.

Static pressure drop values for rigid sheet metal duct types of a specific diameter and flow rate have been well documented. American Society of Heating, Refrigerating and Air-Conditioning Engineers (ASHRAE) published static pressure loss values for this duct type in each ASHRAE Fundamentals (ASHRAE 2005 pp. 34.9)[4]. Static pressure drop values may be acquired using the equivalent roughness or friction factor and the Moody diagram (Moody 1944)[5], The have also been incorporated into tables, charts, and devices, commonly called ductulators (Trane Co.1976)[6], used by contractors to calculate the required size of duct.

Multiple other types of air ducts exist in the market. These include foil-faced duct board, spiral flexible duct, and non-metallic flexible duct. Flexible duct can be compressed, curved, and bent for use in a variety of configurations. The most common current type of flexible duct utilizes a galvanized metal helix with a laminate adhered to each individual helix (Richards 1988)[7]. Due to its flexible nature, many contractors prefer flexible duct because it allows for ease of installation. "Flexible ductwork is used extensively within the residential HVAC market. These systems are generally sized and laid out based upon "rules-of-thumb" either learned through direct experience or passed down through the trades. Poorly designed flexible duct systems perform below the anticipated level of operation" (Kokayko et al. 1996 pp.1)[8]. Flexible duct may be easily routed around obstacles, while rigid duct requires a variety of angled fittings to make the

same turns. Other benefits associated with flexible duct include low cost, sound attenuation and preinstalled duct insulation.

Flexible duct installations also exhibit several potential shortcomings. The duct can be installed with unnecessary compression, or can be forced to make bends that raise the static pressure loss by as much as a factor of 10. Installed compression ratios in new residential construction have been visually observed by the author to vary from 10% compression to over 50% compression. Static pressure loss values for flexible duct do exist, as was published in ACCA Manual D and by manufacturers, but excluding the data taken by Abushakra (Abushakra et al. 2002)[9], these assume ideal conditions such as the duct being fully stretched. The existing data does not include a compressibility factor other than ASHRAE correction factors, making the data difficult to apply to actual installation practices.

Without reliable static pressure drop values, sizing equipment becomes difficult for a designer or an installer using a flexible duct delivery system. A duct system with unknown pressure drops also makes it difficult to effectively balance the air delivery between rooms since the static pressure drop of each component in the system is unknown—a system must be balanced to achieve optimum design (Tsal 1986)[10]. Improper system balance can lead to poor airflow performance of zones served by flexible duct with uncalculated factors.

With the popularity and variability of flexible duct systems, ASHRAE and the Air Distribution Institute (ADI) commissioned this study to quantify the static pressure loss values for non-metallic flexible duct. These values need to reflect the types of

configurations typically seen in common home construction, as well as reflect the static pressure drop for various percentages of compression. The need also exists for an equation which predicts pressure drop in non-metallic flexible duct that includes a provision for compression.

CHAPTER II

LITERATURE REVIEW OF PREVIOUS STATIC PRESSURE LOSS RESEARCH

A literature review of previous duct research was conducted to determine the current level of information regarding pressure loss in flexible duct. The literature was reviewed for duct-related publications from scientific and industry sources. The reviewed publications addressed multiple aspects of duct performance including airflow efficiency, static pressure loss, duct leakage, sound attenuation, and duct system design to determine the existing amount of research. The literature survey covers experiments that have addressed airflow efficiency; two studies (Abushakra et al. 2002[9], ACCA 1995[3]) have published static pressure loss of compressed flexible duct. The studies relating to flexible duct losses are discussed first, with other types of duct-related research following.

Residential air distribution system pressure loss research was conducted at the Lawrence Berkeley National Laboratory (LBNL) (Abushakra et al. 2002)[11]. Abushakra's research found that the published flexible duct calculations (ASHRAE 2005)[4] include error percentages up to 70%, with lower calculated values than the actual pressure drops. He tested 6", 8", and 10" flexible duct on a flat floor at three compression values in a draw-through negative pressure configuration using a draw through configuration with the fan at the outlet. His test configurations included maximum stretch, 15% compressed, and 30% compressed flexible duct. Abushakra also

tested duct board triangle splitter boxes in sizes of 8”x6”x6”, 10”x8”x8”, and 10”x8”x6”, as well as flexible duct 90° elbows in 6”, 8”, and 10”, and supply boots in 6” and 8”. . The testing by Abushakra was conducted according to ASHRAE Standard 120-1999 (ASHRAE 1999)[12]. Standard 120-1999 (ASHRAE 1999)[12] specified testing and measurement of static pressure losses through flexible duct. The Abushakra study provided experimentally determined static pressure loss values for compressed flexible duct.

Similar research was also conducted at Integrated Building and Construction Solutions (IBACOS) for the Burt Hill project (Kokayko et al. 1996)[8]. IBACOS researchers measured the static pressure drop through straight run flexible duct, flexible duct elbows, and triangular duct board plenum boxes. Straight run duct lengths of 25 ft. were tested in fully stretched and 10% compressed configurations. Diameters of 6’’, 8’’, 10’’, and 12’’were evaluated. All testing was conducted with the duct fully supported. Results from the testing showed an increase of pressure loss of 35% to 40% for the relaxed duct work over the fully stretched, with the sheet metal duct experiencing the lowest pressure loss. “The pressure losses associated with the relaxed flexible ductwork were much greater than the losses associated with the taut flexible ductwork” (Kokayko et al. 1996 pp.3)[8].

Elbow testing was conducted by bending sections of flexible duct into “elbows of various radii.” The researchers used peg board forms and wooden dowels to form the duct into the various elbows. Tested radius over diameter (R/D) ratios included 0, 1, 1.5, and 2. Tested diameters were again 6”, 8”, 10”, and 12”. Results of the research

indicated that the "published data for flexible ductwork elbows reasonably approximated the measured pressure losses for all ducts except the 12" diameter (Kokayko et al. 1996)[8]. The IBACOS researchers did not comment on why the 12" diameter behaved differently, but stated that "inconsistency between test procedures may be the source of these differences" (Kokayko et al. 1996)[8].

Triangular terminal box testing was conducted for inlet diameters of 8", 10", and 12". Outlet diameters ranged between 6" and 10". For each combination of inlet/outlet, three sizes of plenum were evaluated: small, medium, and large. A small plenum was defined as having the minimum area for connecting the inlet duct, or 2" greater than the inlet duct diameter. A medium plenum was 4" larger than the inlet duct, and the large plenum was 8" larger than the inlet duct. Results of the testing showed that "fitting pressure losses varied depending upon the inlet/outlet duct geometries and plenum box dimensions" (Kokayko et al. 1996)[8]. The large plenums exhibited the highest pressure losses while the medium plenums exhibited the lowest pressure loss. The IBACOS research determined loss values for minimally compressed flexible duct as well as plenum and terminal boxes. The IBACOS research did not determine static pressure losses for flexible duct compressed greater than 10%.

ACCA publishes *Residential Duct Systems*, or Manual D (ACCA 1995)[3]. This manual addresses sizing of duct systems, and introduces common types of equipment used in residential heating and cooling. Manual D includes static pressure loss charts for non-metallic flexible duct, but does not include compression rate. The pressure loss values for rigid sheet metal are taken from American Society of Heating, Refrigerating,

and Air-Conditioning Engineers (ASHRAE) values published as Chapter 35-Duct Design in the ASHRAE Handbook- Fundamentals (ASHRAE 2005)[4]. ACCA Manual D also includes a friction chart for flexible, spiral wire, helix core ducts, but there are no references available to determine the source of the data included within the chart.

Research conducted by Moody (1944)[5] defined friction factors for flow through pipe and duct given surface roughness. His article, *Friction Factors for Pipe Flow,* appeared in a 1944 *ASME Transactions*. Included in this article were the Moody diagram and an explanation as to how to use it. This diagram allows the user to reference surface roughness and the Reynolds Number to provide the coefficient of friction factor. The friction factor may then be input into the Darcy equation (Eqn. 2.1) to provide head loss (Moody 1944)[5].

$$\Delta P = 12 * f * (L / D_h) * \rho * (V / 1097)^2 \quad \text{(IP Units)} \qquad \textbf{(2.1)}$$

where:
P= Pressure (inH_2O)
f = Friction Factor (dimensionless)
L= Length (ft)
D_h= Hydraulic Diameter (ft)
ρ= Density (lb/ft^3)
V= Velocty (ft/s)

Pressure losses through rigid duct may be calculated using this method, given the value for surface roughness. This work made it possible to calculate the pressure losses through pipe, but not for flexible duct since the internal flow geometry and equivalent

surface roughness of installed flexible duct varies depending on installation configuration.

The Altshul-Tsal equation (Eqn. 2.2) was created to calculate friction factor given material surface roughness, diameter, and Reynolds Number (Tsal 1989)[13].

$$f = .11*(\frac{12*\varepsilon}{D_h} + \frac{68}{\mathrm{Re}})^{.25} \quad \text{(IP Units)} \qquad \textbf{(2.2)}$$

where:
ε = Roughness height (ft)
Re= Reynolds Number (dimensionless)

The equation combines the work of Altshul and Kiselev (1975)[14], and Tsal (1989)[13] to eliminate the use of a chart such as the Moody diagram to determine friction factor. One method currently used involves calculating the static pressure loss with the Darcy equation and applying ASHRAE correction factors for flexible duct. Abushakra's work proved this method to have 20-40% error in some cases (Abushakra et al. 2002)[9]. Unfortunately, no previous work has produced an equation for evaluating the static pressure loss through flexible duct without the use of ASHRAE correction factors.

Research by Harris centered on leakage testing in very early forms of flexible duct. The ducts studied were used for transferring ventilation air within coal mines. Harris conducted several porosity and leakage tests on various types of ducts ranging from woven fabrics to soft plastics to PVC impregnated fabrics (Harris 1958)[15]. Although these ducts differ from the modern type of residential flexible duct utilizing a

galvanized metal helix and Mylar body, one duct that was tested did utilize a flexible plastic outer layer wrapped around a steel helix of two turns per foot. Harris tested leakage at pressures up to 20 inH_2O in duct lengths of 100 ft. with 4 joints per 100 ft. He established a unit-less "leakage coefficient" in order to be able to directly compare ducts of different material types. The leakage coefficient provides a comparative scale of leakage between different duct types, with 0 indicating no leakage. After reviewing the results, Harris established the leakage coefficient for steel duct at 10, though actual tested steel duct leakage coefficients were as low as 2. Resulting flexible duct leakage coefficients ranged from 2.7 up to 387, with 387 being the upper limit of measurement ability. Ducts constructed from sheet plastic or plastic impregnated fabric performed the best, being grouped into a leakage coefficient range of 2.7 to 22.5. The work by Harris provided previously unknown values for leakage and porosity in 25 types of flexible duct, but did not provide any data on the static pressure losses of these ducts.

Other published work focused on duct system design and performance. Work by Bricker in 1961 focused on overall system testing and developing a proportional balancing method with work done in determining independent absolute branch values (Bricker 1961)[16]. However, at this stage in the development of duct system design procedures, modern flexible duct product types had not yet entered the residential market. Harrison published an article in 1965 "concerned with the procedure for regulating or balancing a ventilation system" that discussed several methods and instrumentation (Harrison 1965)[17]. Early measurement methods in residential airflow sought to yield data for balancing methods, not static pressure drop. These design

methods consider the losses throughout the entire duct system for design purposes, but do not provide any methodologies for solving the static pressure loss in flexible duct.

System design methods continue to be created. These include the equivalent length method, the static regain method, the velocity reduction method, and the T-method. Numerous revisions to the static regain method have been published: Fellows in 1939[18], Shieh in 1983[19], and Scott in 1986[20]. The static regain method would later be challenged as false (Tsal 1988)[21]. The T-method development began in 1988 with the publication of an *ASHRAE Transactions* paper (Tsal 1988)[21]. Though the design methodologies continued to change, no published work appeared with the focus of determining flexible duct pressure losses.

The Trane Company published the *Explanation of the Trane Air-Conditioning Ductulator* in 1976. These devices, available for both rigid and flexible duct, make no provisions for using information on the degree of compression in flexible duct.

The literature survey revealed that a need exists for validated experimentally determined static pressure losses in residential flexible duct. The work by Abushakra et al. (2002)[9] determined losses for flexible duct in a negative pressure setup, but did not test a positive pressure blow-through configuration. The IBACOS work (1996)[22] tested compressed flexible duct, but only a 10% compression configuration and did not test the duct using any support other than fully supported. The work by Harris (1958)[15] focused on flexible duct leakage. The Moody diagram (1944)[5] combined with the Altshul-Tsal equation (1989)[13] allows for the calculation of losses through rigid duct, but cannot be used for flexible duct due to the different internal geometry. System design methods

attempt to calculate whole-system losses but cannot be used to calculate the static pressure loss through flexible duct. The values found in ductulators are only applicable to systems at ~4% compression. Static pressure loss values for flexible duct, which include percentage compression and non straight configurations, have not been found in the available published literature. No previous research was found which determined pressure loss values for as-installed flexible ducts.

CHAPTER III

AS-BUILT TEST PROTOCOL

Existing flexible duct installation standards rely on instructions specified by duct manufacturers. The Air Diffusion Council (ADC) produces the Flexible Duct Performance and Installation Standards manual, currently in the fourth edition. Installation standards for both joist-supported and hung configurations state that installation should be done "per manufacturer's installation instruction" (ADC 2003)[23]. This standard leaves the joist-supported installation up to the installer in the event the manufacturer did not include instructions. The ADC standard specifies that hung flexible duct "shall be supported at manufacturer's recommended intervals, but at no greater distance than 5' [1.5m]." Maximum permissible sag is ½" per foot [42mm per meter] of spacing between supports" (ADC 2003)[23], as displayed in Figure 1, representing Figure 10 from the ADC Flexible Duct Performance and Installation Standards. The installation standard does state that "the amount of sag allowed between support joists will have serious effects on system performance due to the increased resistance each introduces" (ADC 2003)[23].

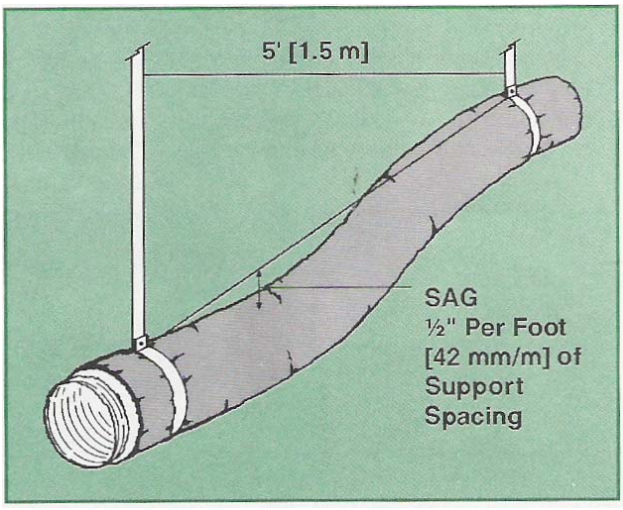

Figure 1. Figure 10, ADC Flexible Duct Performance & Installation Standards, 4th Edition

Experimental testing instructions for flexible duct exist in ASHRAE Standard 120-1999 as Annex E. The standard specifies 110 N of applied tension in static pressure loss testing which nullifies the effect of compression on the data. The standard has no inclusion of hung configuration testing. Installations including hung flexible duct are common in the as-built environment.

Field inspections conducted by Energy Systems Laboratory personnel of as-built new residential homes utilizing flexible duct by reveal a large amount of variability in installation and a lack of adherence to flexible duct manufacturer instruction. Compression ratios of around 30% were observed, as were sag rates exceeding 10" per each 5 ft. section. Additionally, ducts were observed running across attic insulation and constricted up to 30% by hanging supports.

The disparity between the specification put forth in ASHRAE 120-1999 and the features observed in the actual as-built environment led to the creation of an additional

test protocol. This "As-Built Test Protocol" (ABTP) seeks to mimic duct configurations encountered in the built environment in the laboratory in a verifiable fashion. The protocol includes testing flexible duct in configurations that both meet and exceed the requirements set forth in the ADC manual and ASHRAE Standard 120-1999. In this way, a range of resulting values can be developed.

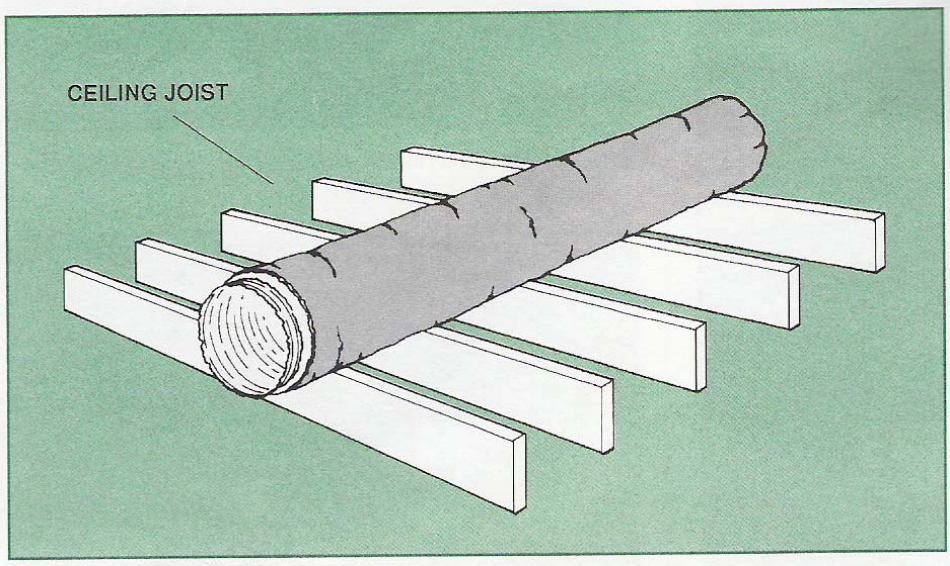

Figure 2. Figure 14, ADC Flexible Duct Performance & Installation Standards, 4th Edition

The configurations chosen for use in the ABTP include both hung and joist-supported configurations. Hung configurations were tested at sag rates of 2", 4", 6", 10", and 16" sag per 5'of support. The sag rate equates to the distance that the duct sags in the center of the supports, or 2.5' from either end, measured from support centerline to duct centerline. Two inches of sag satisfies the ADC recommendation of ½" sag per

foot of support distance as shown in Figure 2, while the other sag rates are indicative of installations seen in as-built construction.

Joist supported configurations were further separated into separate test configurations titled “board-supported” and “joist-supported.” Board-supported configurations were fully supported by a flat surface. The duct was arranged in a straight line, with axial compression throughout. Sag is not a variable in board-supported configurations since the duct receives full support. This configuration replicates duct installations across plywood or flat surfaces.

Joist-supported configurations utilized a test setup designed to replicate attic joists 1.5” wide, detailed further in the *Test Setup* section. This configuration was further separated into “natural sag” and “upper-limit sag” configurations. Natural sag configurations indicate the duct sagging under its own weight with no sag imposed. Upper limit sag replicates conditions where the duct has been installed over time and represents the upper range of loss values. Sag is imposed on the duct with a value of 6” for 30% compressed upper limit sag 6” duct and 10” for 45% compressed upper limit sag. 8” duct upper limit sag values include 6” sag for 30% compressed duct and 9” for 45% compressed duct. 10” duct upper limit sag values were 5” sag for 30% compressed duct and 8” sag for 45% compressed duct. By utilizing these two configurations, a range of results can again be developed to represent as-built conditions.

CHAPTER IV

AIRFLOW THEORETICAL DEVELOPMENT

Measuring the static pressure loss across calibrated flow nozzles within a nozzle chamber quantifies airflow within the system. Conversion of static pressure drop values across the airflow chamber flow nozzles into airflow cubic feet per minute (CFM) takes place in the FlowCalc spreadsheet. This spreadsheet includes all the equations necessary to equate static pressure drop through the flow nozzles to mass flow rate in the system. These equations may be found in ASHRAE Standard 120-1999, Section 9.

ASHRAE produces several calibrated spreadsheets for use in airflow testing. The sheets utilize the same equations listed below. The FlowCalc sheet was created as an alternative to the calibrated ASHRAE sheets. Results from the FlowCalc sheet were compared with the corrected ASHRAE sheets for accuracy and were found to produce identical results.

Inputs (IP) [SI]

A = Area, (ft^2) [m^2]
A_n = Nozzle throat area, (ft^2) [m^2]
C_n = Nozzle discharge coefficient, dimensionless
D = Nozzle diameter, (in.) [mm]
d = Nozzle throat diameter, (in.) [m]
$L_{x\text{-}x'}$ = Length of duct between planes, (ft) [m]
P_b = Barometric Pressure, (inHg) [kPa]
Note: Recorded by monitor program.
P_e = Saturated vapor pressure of ambient air, (inHg) [kPa]
P_p = Partial vapor pressure of ambient air, (inHg) [kPa]
P_5 = Static pressure recorded before nozzle bank, (inH_2O) [Pa]
Note: Recorded by monitor program.

Q = Volume flow rate, (ft/min) [L/s]

R = Gas constant, ($ft\text{-}lb_f/lb_m\text{-}^oR$) [kJ/kg-ºK]

Re_d = Reynolds number at nozzle throat diameter, dimensionless

T = Temperature, (ºF) [ºC]

T_5 = Dry-bulb temperature of air upstream of nozzles, (°F) [°C]
Note: Recorded by monitor program.

T_{wb} = Wet-bulb temperature of air within laboratory, (°F) [°C]
Note: Calculated

T_{amb} = Ambient temperature within laboratory at time of test, (°F) [°C]
Note: Recorded by monitor program.

V = Velocity, (ft/min) [m/s]

Y = Nozzle expansion factor, dimensionless

ΔP_{noz} = Static pressure difference across nozzle, (inH_2O) [Pa]
Note: Recorded by monitor program.`

α = Ratio of absolute nozzle pressure to absolute approach pressure, dimensionless

μ = Dynamic viscosity of air, ($lb_m/ft\text{-}s$) [Pa-s]

ρ = Air density, (lb_m/ft^3) [kg/m^3]

Calculations

The following calculations determine atmospheric air density given dry bulb temperature, wet bulb temperature, and barometric pressure. The air density must be taken in the test area. The saturated vapor pressure of the ambient air within the test area is:

P_e Saturated Vapor Pressure. (inH_2O) **(4.1)**

(IP) $= (2.96 * 10^{-3}) * (T_{wb}{}^2) - (1.59 * 10^{-2}) * T_{wb} + .41$ (inH_2O)

(SI) $= (3.25 * 10^{-3}) * (T_{wb}{}^2) - (1.86 * 10^{-2}) * T_{wb} + .692$ (kPa)

The partial vapor pressure of the water in the air can then be found as:

P_p Partial Vapor Pressure. **(4.2)**

(IP) $= P_e - (P_b * ((T_{amb} - T_{wb}) / 2700))$ (inH_2O)

(SI) $= P_e - (P_b * ((T_{amb} - T_{wb}) / 1500))$ (Pa)

and the density of the air within the test space with

ρ_o Ambient Density of air within laboratory. **(4.3)**

(IP) $= 70.75 * (P_b - .378 * P_p) / (53.35 / (T_{amb} + 459.7)$ (lb/ft^3)

(SI) $= (P_b - .378 * P_p) / (.287 / (T_{amb} - 273.2)$ (kg/m^3)

From the ambient density the chamber density may be calculated.

ρ_5 Density of air within flow measurement station (nozzle chamber). **(4.4)**

(IP) $= \rho_o * ((T_{amb} + 459.67) / (T_{db} + 459.67) * ((P_{noz1} + 13.63 * P_b) / (13.63 * P_b))$ (lb/ft^3)

(SI) $= \rho_o * ((T_{amb} + 273.2) / (T_{db} + 273.2) * ((P_{noz1} + 1000 * P_b) / (1000 * P_b))$ (kg/m^3)

Gas constant:

R Gas constant of air at around 70° F **(4.5)**

(IP) $= 53.35$ $(\frac{ft * lbf}{lbm * R})$

(SI) $= .287$ $(\frac{kJ}{kg * K})$

The ratio of absolute nozzle exit pressure to absolute approach pressure is calculated using the ΔP across the flow nozzles as well as the gas constant, dry bulb temperature and air chamber density.

A Alpha ratio **(4.6)**

(IP) $= 1 - (\Delta P_{noz}) / (P_5 + 13.63 * P_b)))$

(SI) $= 1 - (\Delta P_{noz}) / (P_5 + 1000 * P_b)))$

The viscosity of the air flowing through the nozzle chamber and test section may be assumed as a constant for temperatures between 20ºF and 110ºF (-4ºC and 32ºC).

μ Dynamic air viscosity **(4.7)**

(IP) $= 1.222E^{-05}$ $(\frac{lbm}{ft * s})$

(SI) $= 1.819E^{-5}$ (Pa*s)

The expansion factor of the air leaving the flow nozzles is used to quantify the interactive pressure change of the air and the flow nozzles,

Y Expansion factor **(4.8)**

(IP) $$= \left[3.5\ \alpha^{1.43} \left(\frac{1-\alpha^{0.286}}{1-\alpha} \right) \right]^{0.5}$$

(SI) $$= \left[3.5\ \alpha^{1.43} \left(\frac{1-\alpha^{0.286}}{1-\alpha} \right) \right]^{0.5}$$

and using the expansion factor, the Reynolds Number of the air within the chamber is determined:

Re Reynolds Number of air within chamber **(4.9)**

(IP) $= 1{,}363{,}000\,(d/12)\,(\rho_5\ \Delta P_{noz})^{0.5}$

(SI) $= 70{,}900\ d\ (\rho_5\ \Delta P_{noz})^{0.5}$

then the discharge coefficient can be determined.

C Discharge Coefficient **(4.10)**

(IP) $$= .9965 - .00653 * \sqrt{\frac{10^6}{\mathrm{Re}}}$$

(SI) $$= .9965 - .00653 * \sqrt{\frac{10^6}{\mathrm{Re}}}$$

The product sum of each discharge coefficient used in the nozzle chamber is next to be determined. Each nozzle has a separate discharge coefficient and area, and these must be summed up to quantify the coefficient of the overall chamber.

ΣCa Sum of coefficients.

$$= D_{n1} * C + D_{n2} * C + ... + D_{ni} * C \qquad \textbf{(4.11)}$$

Then, using the discharge coefficient, the volumetric amount of airflow passing through the nozzle bank and into the system may be determined.

V_{dot} Volumetric flow rate (ft^3/min) [l/s] **(4.12)**

(IP) $$= 1096 * Y * \sqrt{\frac{\Delta P_{noz}}{\rho_o} * \Sigma Ca} \qquad \left(\frac{ft^3}{\min}\right)$$

(SI) $$= 1096 * Y * \sqrt{\frac{\Delta P_{noz}}{\rho_o} * \Sigma Ca} \qquad \left(\frac{l}{s}\right)$$

Using the duct diameter, the area of the duct under test may be calculated,

Dd Diameter of duct under test (ft^2) (m^2) **(4.13)**

Ad Area of duct under test **(4.14)**

and by using the duct area and volumetric flow rate, the velocity of the air in the duct may be determined.

Vd Velocity of air within duct under test **(4.15**)

$$= \frac{V_{dot}}{A_d}$$ *(ft/min) (m/s)*

CHAPTER V

TEST SETUP

A data acquisition (DAQ) setup was used to control and record the static pressure drop of airflow through the duct test section and nozzle chamber. Computer controlled cooling coils and electric resistive heater devices could modify the thermal properties of the air to maintain constant values during an experimental run. The system utilizes computerized data collection along with fully adjustable rates of airflow and heat input. For the purposes of this study, ambient air conditions were used as per ASHRAE request; however, the test setup includes the capability to condition the air when required.

A 5-ton Lennox residential blower cabinet and cooling coil supply conditioned the air for testing when required. Temperature could be controlled from 55°F up to 100°F, using an electric resistance heating coil in a blow-through reheat configuration. Both temperature and flow rate were monitored and controlled from the data acquisition (DAQ) system. This system has the capability to control the air to 70°F (±1°F) and 50% RH (±5% RH), and to measure the air to ±1°F and ±2% RH. Figure 3 displays a diagram of the test setup. Although not required by ASHRAE Standard 120-1999, this level of control can increase the consistency of the unprocessed data. ASHRAE Standard 120-1999 requirements were used to process the data after acquisition.

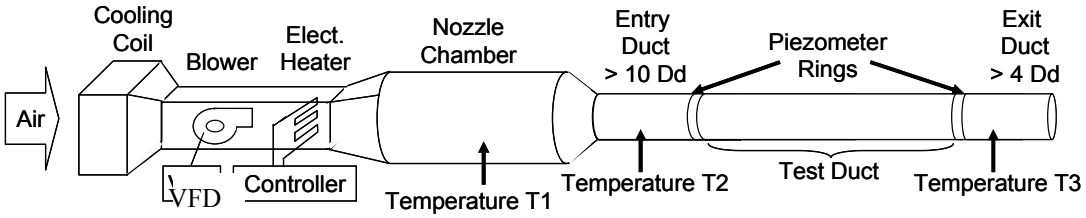

Figure 3. Test setup diagram (Culp 2005)[24]

A computer controlled variable frequency drive (VFD) adjusts the airflow. The VFD provides for varying the fan RPM to provide a range of 50 to 1500 CFM. A voltage signal produced from one of the analog output channels of the DAQ card controls the VFD. It then delivers an operating RPM proportional to that voltage. The amount of reheat also feeds through the DAQ card to the Triac heater controller. The Triac, when required, controls the heater to deliver heat proportional to a voltage selected by the user.

Sensor	Manfr.	Model	Element	Range	Unit	% Accuracy (+/-FS)	Drift	Output	Response Time (mS)
Δ Pressure	Dwyer	607-0	Silicon Diaphram	0:.1	inH_2O	0.25%	.5% FS/yr	4:20 mA DC	250
Δ Pressure	Dwyer	607-1	Silicon Diaphram	0:.25	inH_2O	0.25%	.5% FS/yr	4:20 mA DC	250
Δ Pressure	Dwyer	607-21	Silicon Diaphram	0:.5	inH_2O	0.50%	.5% FS/yr	4:20 mA DC	250
Δ Pressure	Dwyer	607-3	Silicon Diaphram	0:1	inH_2O	0.50%	.5% FS/yr	4:20 mA DC	250
Δ Pressure	Dwyer	607-4	Silicon Diaphram	0:2	inH_2O	0.50%	.5% FS/yr	4:20 mA DC	250
Temperature	Dwyer	650-2	Silicon Junction	20:120	°F	0.30%	.5% FS/yr	4:20 mA DC	500
				Humiditiy: 0:90%		2%			
				Humidity: 90:99%	%RH	2%+1%M			
Temp/RH	Vaisala	HMD60Y	Humidcap/Platinum	Temperature:20:80	°C	.6 °C		0:10 V	15000

Table 1. Sensor Specifications

Figure 4. Test setup data acquisition system (DAQ)

Fan speed control regulates the airflow volume between 50 CFM and 800 CFM. An array of Dwyer Series 607 pressure transducers with an accuracy of ±0.25% FS for pressure drops of up to 0.25" inH_2O and ±0.5% FS for pressure drops from 0.25" inH_2O to 2.00" inH_2O measure the pressure drop through the corresponding duct or fitting. These 4 – 20 mA transducers produce a current in proportion to the amount of applied pressure. A 249.0 Ω precision resistor (±0.25%) converts the current loop outputs from the sensors to voltage inputs to the DAQ. Sensor specifications may be viewed in Table 1. The DAQ processes the voltages and the program in the computer performs the requisite calculations and display functions. A panel provides protection from dust for the pressure transducers and electronics used for conversion, but the pressure transducers are each housed in a NEMA 1 case. The DAQ system is displayed in Figure 4, ,and a circuit diagram for the full system is available in Figure 5.

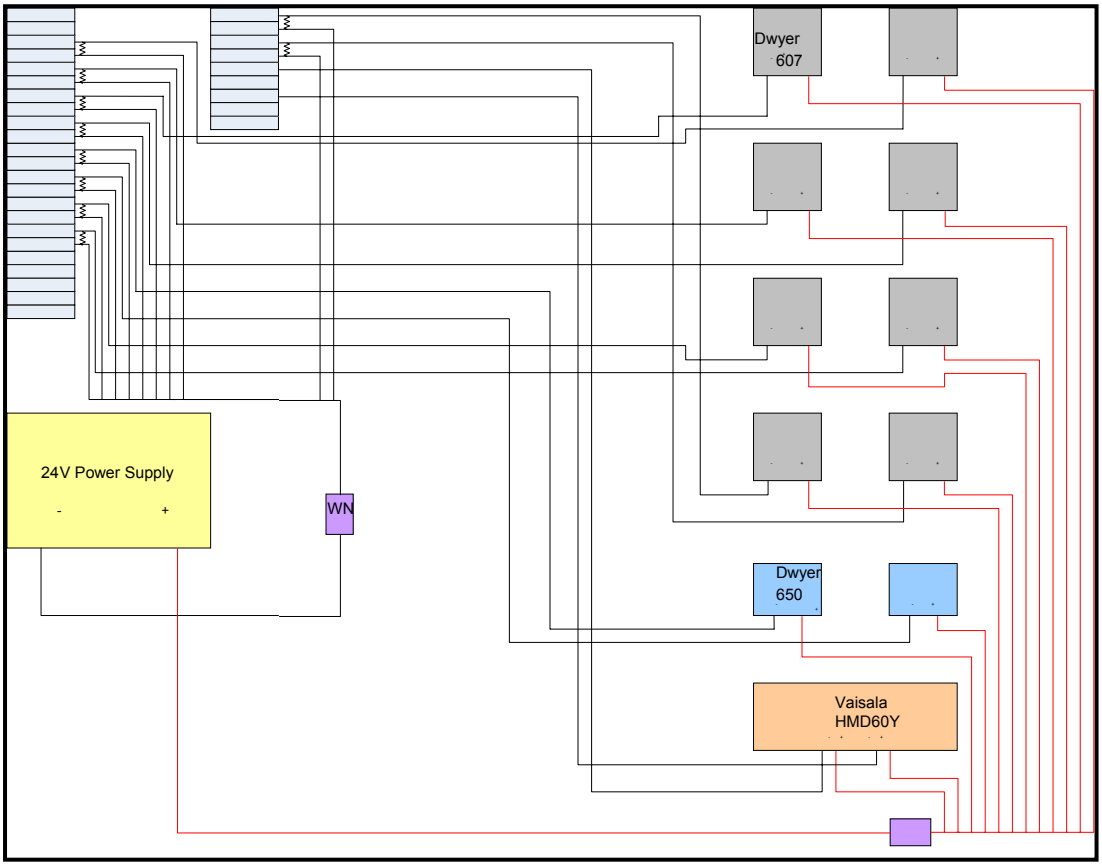

Figure 5. Test setup circuit diagram

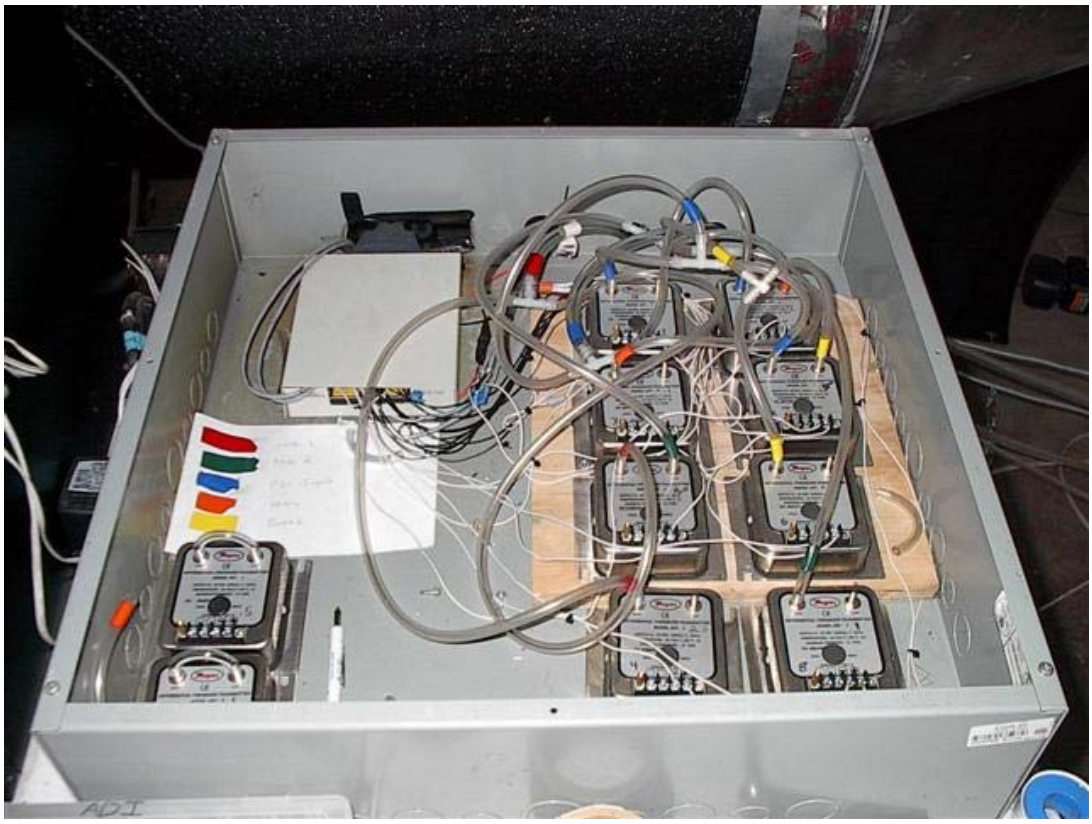

Figure 6. Static pressure sensor array and DAQ input block

The static pressure sensor array is shown in Figure 6. The pressure measurement in the test duct occurs through pressure taps set up in piezometer rings, as constructed to specification in ASHRAE Standard 120-1999, Section 6, Figure 4. The rings function as static pressure averaging devices. Each piezometer ring utilizes four equally-spaced static pressure taps around the circumference of the test duct. The output air tubing of each tap connects into its neighbor. In this manner, any small variation between pressure taps averages out. ASHRAE Standard 120-1999 requires that each tap within the ring record a static pressure value ±2% in reference to one another, be spaced 90° around the circumference of the duct from one another, and sit on the same cross-

sectional duct center line. The piezometer rings used in this experiment satisfy the requirements set forth in ASHRAE Standard 120-1999.

The rings were constructed from 24-gauge copper plate and ¼" inner diameter copper tubing. Copper plates provide excellent malleability along with the ability to shape to various duct curvature. The copper tubing provides a tight seal when covered with 1/2" silicone tubing. Both materials are readily available.

The copper sheet was cut into rectangles measuring approximately 3" x 3". This size provides enough distance to shape to duct curvature while still fitting all four taps around a 6"duct. A sheet metal brake works well for cutting the sheet. The copper tubing was cut into several 1" lengths using a tubing cutter. The cut raw materials may be viewed in Figure 7.

Figure 7. Raw materials for piezometer ring tap

Next, the tubing ends were soldered to the copper sheet segments. These tools included a small torch, brazing alloy, and a pair of pliers for moving the extremely hot, newly soldered segments. A small container was filled with water in order to be used as a quenching tank. Soldering tools can be viewed below in Figure 8.

Figure 8. Soldering tools

The copper tubing sections were soldered into the center of the copper segments, making sure of a sealed connection around the periphery of the tubing. The soldering alloy was first inserted into the tubing section and held perpendicular to the copper sheet. Heat was applied onto the base of the tubing until flux melts and runs out the bottom of the tubing. Heat and brazing alloy were removed, leaving tubing affixed to the sheet

segment. Heat was applied around the tubing until solder thoroughly filled the void between the tubing and the sheet. Figure 9 displays a picture of this process.

Figure 9. Soldering of copper tubing

When the tubing bonded to the sheet, the newly formed tap was quickly dropped into the quenching tank filled with water. The water in the tank need not be cooler than room temperature, and requires immersion time less than one minute. This ensured that the copper sheet remained soft and malleable. Quenching also removed residue from the sheet, providing for adhesion when the taps are taped over. The newly built taps are shown in the quenching tank in Figure 10. Notice the residue floating on the surface of the water.

Figure 10. Quenching tank

Using a 1/8” drill bit, the center was drilled out of the copper sheet sections through the copper tubing sections. This center tap orifice size was consistent with the requirements specified in ASHRAE Standard 120-1999. Mounting the drill bit into a press provides a secure method of drilling, as shown in Figure 11. It was important to drill perpendicular to the copper sheet in order to avoid a slanted hole. A scrap wood block was placed below the tap so that the drill bit passed through the copper sheet and into the wooden block. This was useful in drilling a clean hole and preventing the tap from spinning in the chuck.

Figure 11. Drilling the 1/8" hole in the copper sheet

After the taps were drilled, the backside of the hole contained rough burrs and edges that could potentially foul the measurement. To remove these burrs the backside of the segment was brushed using a wire wheel. Once the taps were brushed and the holes were blown clear, they were complete and ready for installation. Figure 12 displays a completed tap.

Figure 12. Completed piezometer ring tap

When applying the individual taps to the duct, a small ring of silicone sealant was applied first in a 2" diameter circle around the tap hole. This sealant ensured bonding to the ductwork and provided a redundant airtight seal. It was made sure that the sealant did not enter the center hole. The tap was mounted over the hole in the duct section, centering the hole in the tap with the hole in the duct. Foil-faced tape was applied to all four sides of the tap, and the applied tape was smoothed over to remove air bubbles and pockets. A second layer of tape was applied to ensure a positive seal. A complete and installed piezometer ring is shown in Figure 13.

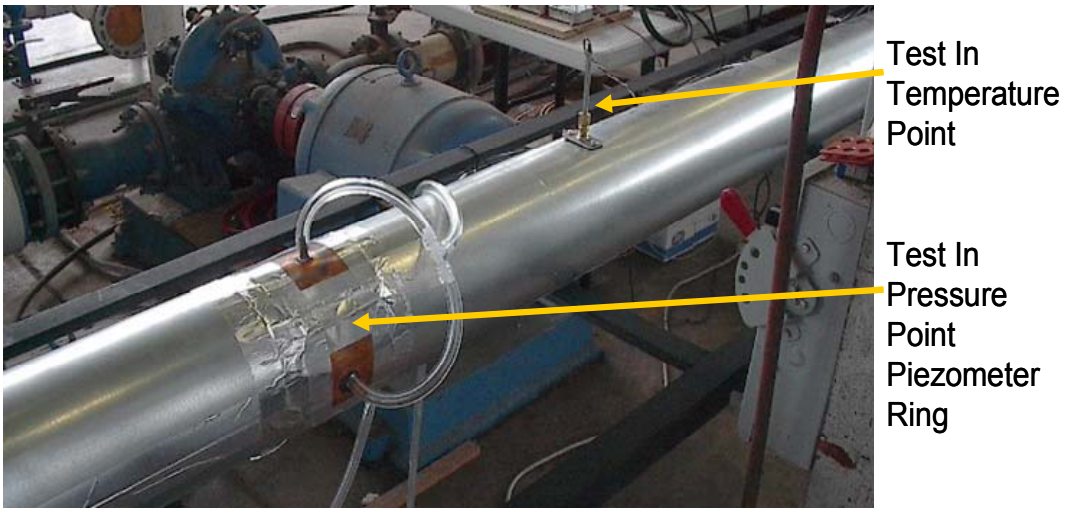

Figure 13. Piezometric ring and temperature sensor

The completed piezometer rings were checked to ensure that they satisfy the requirements of ASHRAE Standard 120-1999, section 6.2. The standard states that each tap must measure within ±2% of the others in the ring. To check the pressures of each tap, three of the four taps were sealed off using short lengths of tubing with one end plugged with silicon sealant. The pressure line was connected to the remaining tap. Once a set of ten data points reported by that tap were recorded, the taps which are sealed off were then rotated. A set of ten data points were then recorded for each connected tap. The average for each tap was taken, and the averages were compared. A satisfactory ring's measured averages are within ±2% of one another, per the requirements of ASHRAE Standard 120-1999. If one or more taps averaged outside of the requirements, then the tap must be checked and possibly reconstructed.

The temperature measurement throughout the test run uses two silicon junction transistor type devices, and a third 1000 Ω combination platinum temperature-humidity unit located in the nozzle chamber. Sensor locations are: 1) at the nozzle chamber; 2) at the beginning of the test section; and 3) at the end of the test section. The temperature sensor location at the nozzle chamber contains the relative humidity sensor. This type of temperature sensor was chosen for its low drift, high degree of accuracy, and response time.

All sensors were calibrated to NIST-traceable devices. The temperature sensors were calibrated by the manufacturer prior to shipment, and then re-calibrated at a 1 year interval using two witness thermometers. The pressure transducers were calibrated by the manufacturer prior to shipment, then recalibrated at a 1 year interval using two witness manometers. The humidity sensor was calibrated by the manufacturer prior to shipment, then re-calibrated at a 1 year period by shipment back to manufacturer.

The pressure drop through nozzles housed in a nozzle chamber quantifies the amount of airflow through the system. Static pressure measurements within the nozzle chamber use Dwyer differential pressure sensors to capture the static pressure change across calibrated precision flow nozzles. The nozzle chamber was constructed by the author to specifications set forth in Section 7 of ASHRAE Standard 120-1999. The chamber utilizes two flow nozzles, a 2.5” and a 5”. The nozzles are ANSI-24c compliant using a low beta ratio design as specified in Section 6 of ASHRAE Standard 120-1999. Galvanized steel (16 gauge) makes up the actual shell of the chamber. The steel was cut into two sections, and the ¼” steel nozzle plate was inserted into the center.

The chamber uses six flow straighteners made from perforated steel. The perforations are ½" in diameter, equally spaced. The straighteners were welded perpendicularly into the shell of the chamber, each equally spaced 2" from one another. Figure 14 displays a diagram of the chamber.

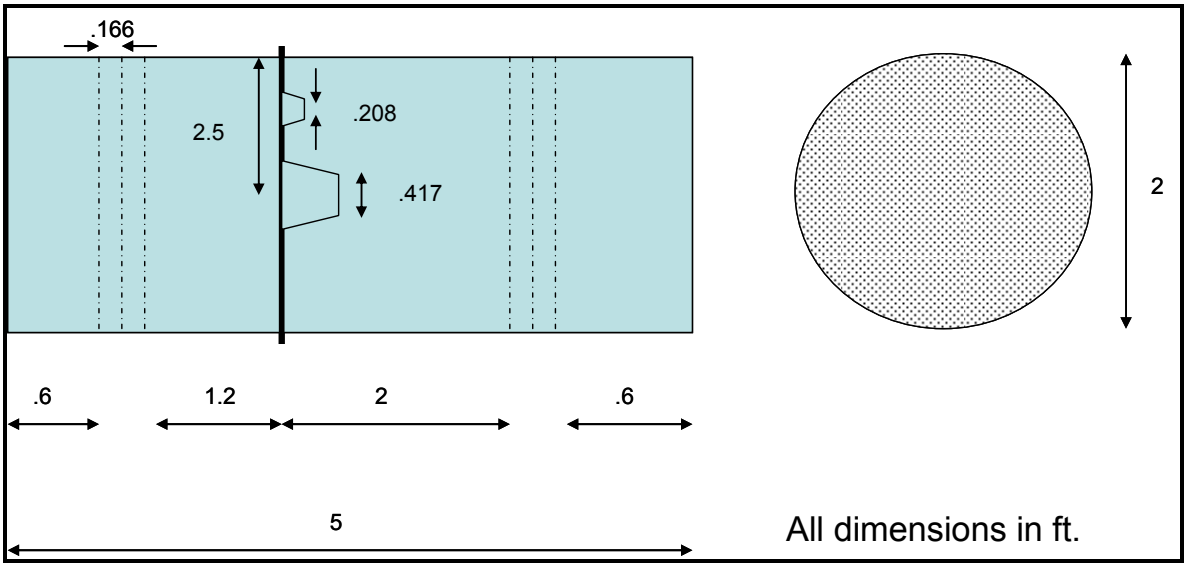

Figure 14. Nozzle chamber

A 14" x 18" access door was cut into the chamber to allow nozzle access. The seams around the door use a rubber weather stripping in conjunction with silicone sealant to make the door airtight. The chamber received a rubberized coating after completion to fill any surface leaks, and to improve the aesthetics and durability of the unit. Twenty gauge galvanized steel transitions were designed by the author and created by M&M Sheet Metal to transition the air from the cooling coil to the blower cabinet, and then from the blower cabinet to the nozzle chamber. These transitions ensure that

maximum blower capacity may be captured for use in the test system. The chamber uses three interchangeable nose cones to deliver the air into the head duct. These nose cones allow the chamber to be adapted to duct sizes of 6", 8", and 10" duct. The nozzle and transitions are shown in Figure 15.

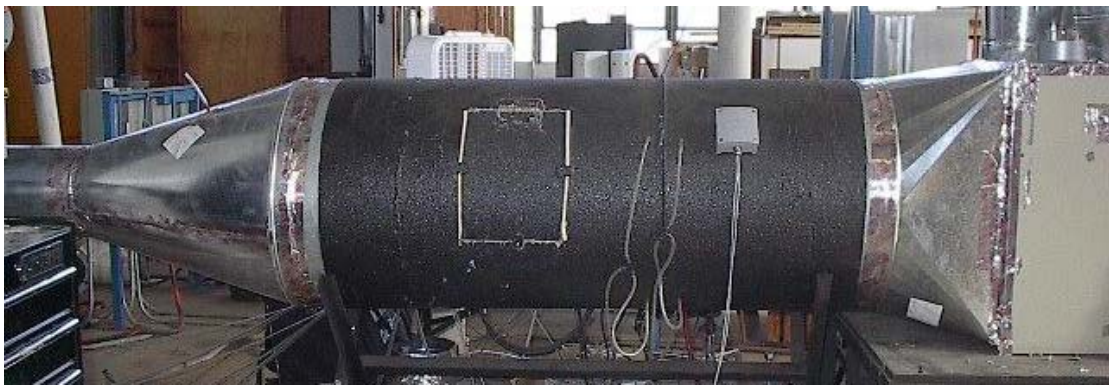

Figure 15. Nozzle chamber and associated transition pieces

A test section support rack holds the test duct. The rack uses 1.5" metal supports spaced every 24" to mimic 2" x 4" attic joists, as seen in Figure 16. These supports provide the forms for the joist-supported testing. The rack sits on four height-adjustable legs. These legs allow the rack to be leveled both longitudinally and horizontally, and to be adjusted vertically to support different duct sizes. 1/8" thick pegboard was cut into 2'x 8' lengths to fit the top surface of the rack. This pegboard has dual uses: it functions as the flat support surface for board supported testing, and with the addition of forms, functions to replicate hung configurations. The forms serve to create a "pathway" which the duct must route through. In this way, test configurations can be defined, providing experimental validity.

Figure 16. Test section support rack

A visual basic software control program displays all values that the system monitors and controls in the system monitor window. The program window allows direct user interface and control. It includes display of the incoming data, as well as adjustable control bars for adjusting the VFD and Triac heater controller. Within the program, the incoming voltages from all sensors are converted from measured electrical signals to numeric digital values. This equipment's automated measurement control acquires 5,000 readings for each point reported. This occurs by taking 100 readings each second and calculating the average of those 100 readings. Next, this process repeats fifty times with each of the fifty point values stored on disk. Retained data includes time and date, as well as chosen measured variables. These variables include temperature and pressure above and below the test section, differential pressure across

the test section, and airflow chamber pressure. This data serves as the raw data for all further analysis. All fifty recorded data points for each flow rate are retained, then averaged to provide one set of values for each flow rate point. The original fifty points may be checked at any time for statistical validity or potential problems. The average sets are combined and processed to provide the final data. Figure 17 displays a block diagram of the system operation.

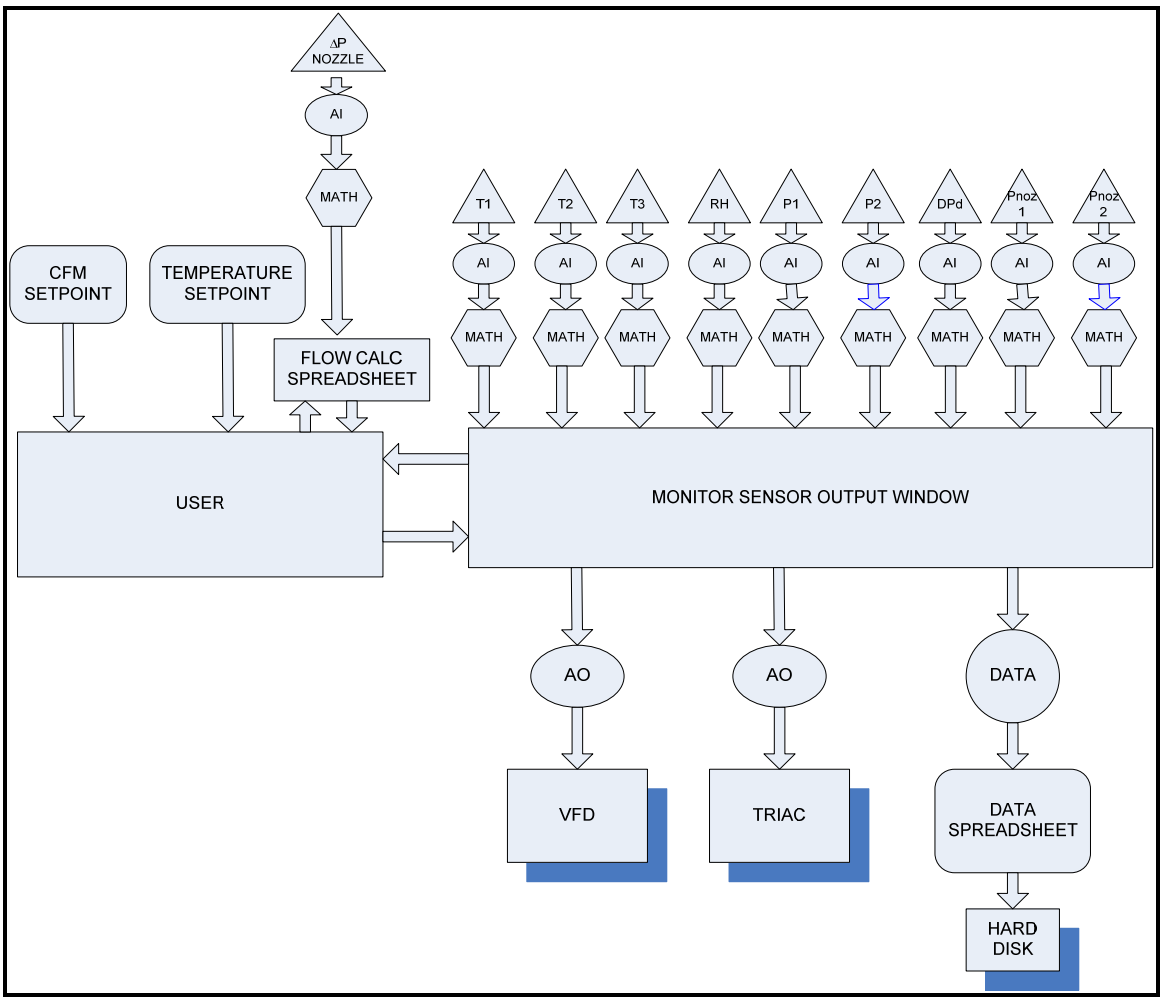

Figure 17. System operation block diagram

CHAPTER VI

DATA ACQUISITION AND OPERATION SOFTWARE DEVELOPMENT

Operation of the test setup required four independent programs and spreadsheets. These consisted of the main operation monitor window interface, in Visual Basic format, and several spreadsheets used for taking data. Appendix A includes a full display and description of the operating code. The operation interface was titled "Monitor Sensor Output." Requirements included the ability to read all of the test sensors sequentially and convert the reported voltages into actual values for the user. The monitor sensor output program also needed to allow the user to export and save the captured data, as well as control external devices such as the VFD and Triac heater controller. Figure 18 displays the monitor window interface constructed for this experiment.

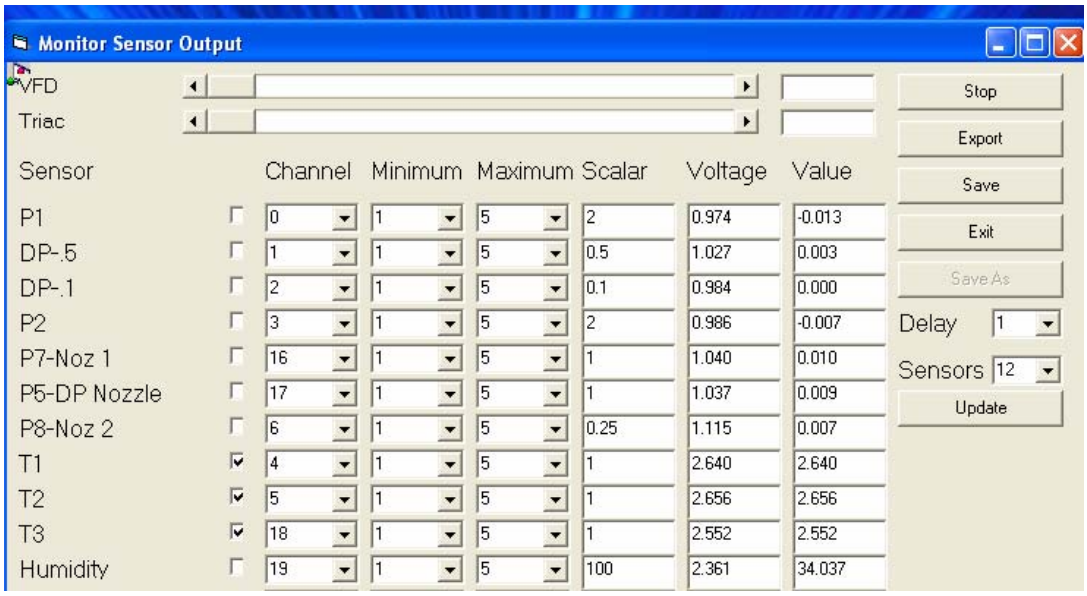

Figure 18. Monitor sensor output window

Modulation controls for the VFD and Triac output voltages were integrated into the monitor window in the form of dual slide bars. Indicator boxes to the right of the slide bars display voltage output to the VFD and Triac control. The monitor displays sensor outputs, and includes buttons for exporting and saving the captured data into spreadsheet format. The data output time step command, in seconds, resides below these buttons. A combination scan/stop button allows the user to discontinue sensor scanning in order to modify the sensor configuration, and then continue capturing data.

The monitor offers user-customizable sensor descriptions. These sensor descriptions, along with channel settings, and voltage range may be changed by the user at any time. The exported data records and reflects these changes. In this way, the monitor may be adapted to numerous experiment types and sensor variations.

Necessary operation spreadsheets included the Test Verification Sheets (TVS). The TVS included the FlowCalc sheet, which utilizes the air property and flow equations discussed previously in the *Air Flow Theoretical Development* section, as well as the test setup sheets. The test setup sheets allow the user to document details and critical manual measurements of the various test configurations. Each TVS includes a simple diagram to assist the user in recording the proper measurements. An example of the straight run test verification sheet is shown in Figure 19.

Date:	**November 13, 2005**		
Tester Name:	**Kevin Weaver**		
Test Duct Size (In.)	**6**		
Test Duct Type:	**Flexible**		
Test Compression	**45.00%**		
Test Configuration:	**45% Joist Supported, natural**		
Test Flow Range (CFM):	**70:200**		
Test Flow Range Interval (CFM):	**10**		
Applicable Pictures:	**HP**		
Ambient Initial Lab Temperature (°F):	**66.9**		
Ambient Final Lab Temperature (°F):	**66.9**		

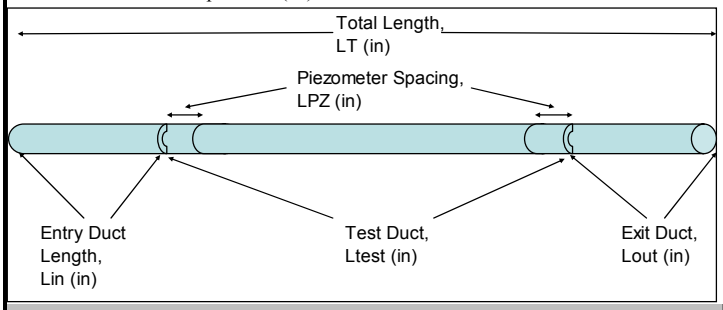

			Explanation
L_{in} (in)	**165**		Length of entry duct from nose cone end to ring 1 (in)
Number Diameters (minimum 10)	**27.50**		
L_{out} (in)	**222**		Length of exit duct from ring 2 to exit (in)
Number Diameters (minimum 4)	**37.00**		
$L_{test,\ max}$ (in)	**292.0**	24.3	Ring to ring distance
Flex Test (in)	268.00		Subtract out LPZ1(14"), LPZ2 (12") and spacer(12").
Flex Test (ft)	22.33		
Flex Test, Compressed (ft) **(DIV)**	12.28	3.36	Length of compressed flex in run (ft.)
Ltest,Compressed (ft)	14.28		Ltest, compressed (compressed ring to ring)
Ltest,Compressed (in)	171.40		
Number Diameters (minimum 25)	28.57		
Ltest,compressed+Lin (ft)	28.03	6.6	Ltest, compressed + Lin
L_{PZ} 1 (in)	**12**		Distance of the Piezometer Ring duct (about 12" or 14")
L_{PZ} 2 (in)	**12**		
Spacer (in)	**0**		
L_T (ft,in)	**639**		
Check	558.40		

Figure 19. Straight run Test Verification Sheet (TVS)

The FlowCalc sheet serves to allow user input of measured and collected air property values in order to produce mass flow rate, given the static pressure drop across the calibrated flow nozzles. The FlowCalc program functions as the user's indication of volumetric flow rate within the system. By using the FlowCalc sheet and operation sheets simultaneously, a user controls and monitors the flow rate through the system and the associated static pressure drop of the duct test section.

CHAPTER VII

EXPERIMENTAL PROCEDURE

Assembling Test Configuration

Prior to the actual collection of data several steps were taken to ensure the integrity and validity of the data. First, the desired test configuration was assembled, being careful to conform to the requirements of Standard 120-1999. It was ensured that all longitudinal and lateral joints were taped, and then smoothed to eliminate any ripples within the tape. The lateral joints then had a second wrap of tape applied, and this wrap was smoothed as well. It was ensured that the run was straight, and that any sag was distributed equally along the length of the test section. This was accomplished by first marking the fully stretched duct into equal 1' sections. Next, these sections were each compressed the desired amount. The overall test section length was checked to ensure correct compression.

System Leak Testing

After the configuration was fully assembled and sealed it was leak tested. The leak test procedure included testing the nozzle chamber, transition piece, and duct section as one system.

1. The test began by opening the nozzle chamber access door to gain access to the downstream ends of the flow nozzles. The nozzle ends were then covered with the nozzle caps. Tape was wrapped around the caps until they created an air-tight seal against the flow nozzles. This prevented air from escaping to the upstream end of the chamber.

2. Any terminal ends of the duct system were then sealed. For straight run testing this was one end, for diverging flow fittings, two. A cut piece of cardboard, foam or other material was used to cover most of the cross-sectional area, then tape was used to seal the periphery and any gaps.

3. The high pressure compressed air line was connected from an available air compressor to the input connection of the Victor flow meter. The output side of the flow meter should connect into a brass fitting in the nozzle chamber.

4. The Sensor Monitor Output window was then opened and "Scan" was selected to begin reading the current static pressure in the chamber, Pnoz2. The pressure will read 0.0 inH_2O with no input into the chamber.

5. The maximum allowable leakage rate for the current test configuration was determined. ASHRAE Standard 120-1999, Annex D states that leakage should be less than ½% of the minimum flow rate to be tested. The equivalent flow rate was determined on the Victor flow meter. The flow meter lists flow in terms of cubic feet per hour, or CFH. The value was divided by 60 to determine the flow rate in units of CFM.

6. The valve on the flow meter was opened to begin to introduce air into the sealed system. The pressure in the system should begin to rise as air is introduced. The airflow was increased until a pressure of 25 Pa, or 0.1 inH_2O was reached. The flow rate was recorded and required to reach this pressure (25 Pa or 0.1 inH_2O) and it was then determined if it met the maximum leakage requirements.

7. If the system could not reach the required pressure leaks that exist in the system, the use of residential leak testing smoke bombs was recommended for pin-pointing leaks in the system. The leaks were located, sealed and the system was retested.

Test Configuration Verification and Documentation

Once the desired configuration is assembled, it must be documented and verified. The Test Verification Sheet (TVS) was used to record the critical measurements and values for checking the configuration for standard validity. The test verification sheet was designed to ensure that any assembled configuration conforms to the requirements

set forth in ASHRAE Standard 120-1999, and to document testing for any required future reference. It was important that all fields were completed on the test verification sheet, and all measurements were completed independently. Each row within the test sheet included descriptions of the required quantities. The test verification sheet was then checked to ensure that the requirements of ASHRAE Standard 120-1999 were satisfied. The test verification sheet was accompanied by a series of photographs capturing the test configuration. The pictures needed to display the compression ratio, sag between joists, and overall form of the compression. The pictures also needed to include a visible reference such as a tape measure or ruler.

The test procedure for joist and board supported configurations followed virtually the same procedure. The first step involved assembling the desired test configuration, then leak testing the pressure lines, nozzle chamber, and test duct. Leak testing used a calibrated regulator/flow meter and compressed air. The airflow fed into the duct or chamber at a set flow rate until the pressure within the vessel reached steady state. The steady state measured airflow equaled the quantity of air leaving the system, which defined the system leakage. Acceptable limits are set forth in *Annex D-Leakage Measurement* of Standard 120-1999 (*ASHRAE 1999*).

The operation of the test system is based around the monitor sensor output window shown in Figure 20. This section will reference many of the buttons and objects shown in the figure, and take the user through the operation in a step-by-step basis.

1. First, the DAQ PC was booted up, and the program entitled “Visual Basic Monitor” was opened. An example of the monitor is shown in Figure 20. The user pressed the forward button, located on the VFD local panel shown in Figure

21, and moved the VFD slide bar, located in the Monitor Sensor Output window, to the middle of its range. This caused the blower to start and ramp up, and the system to pressurize. Pressing the Scan button allowed the user to begin reading the sensors.

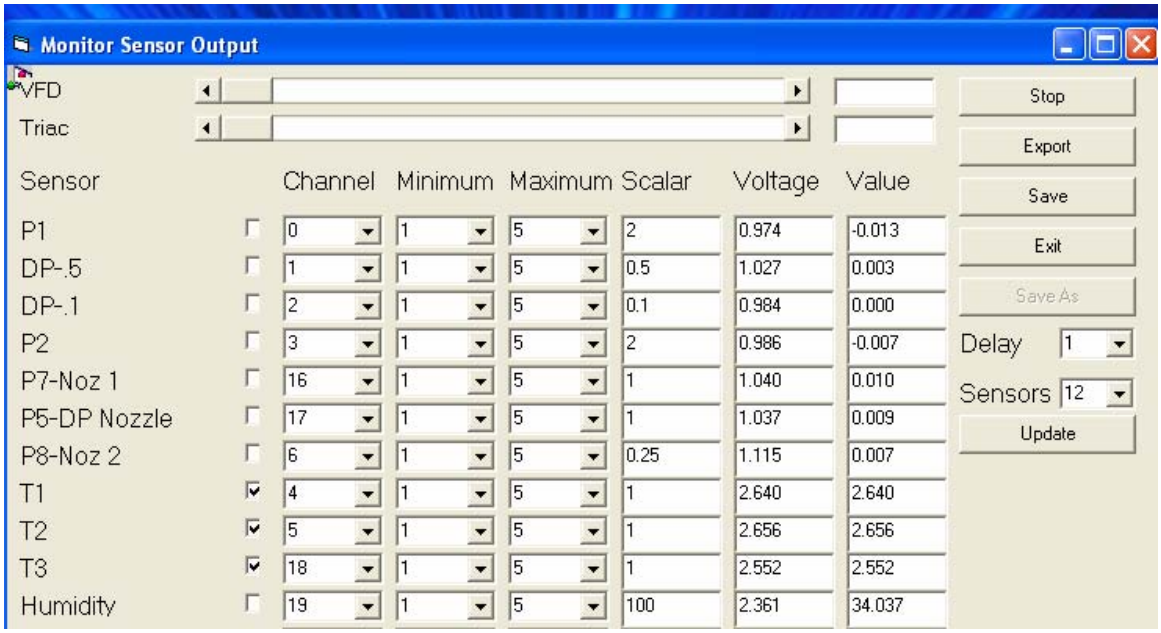

Figure 20. Monitor Sensor Output

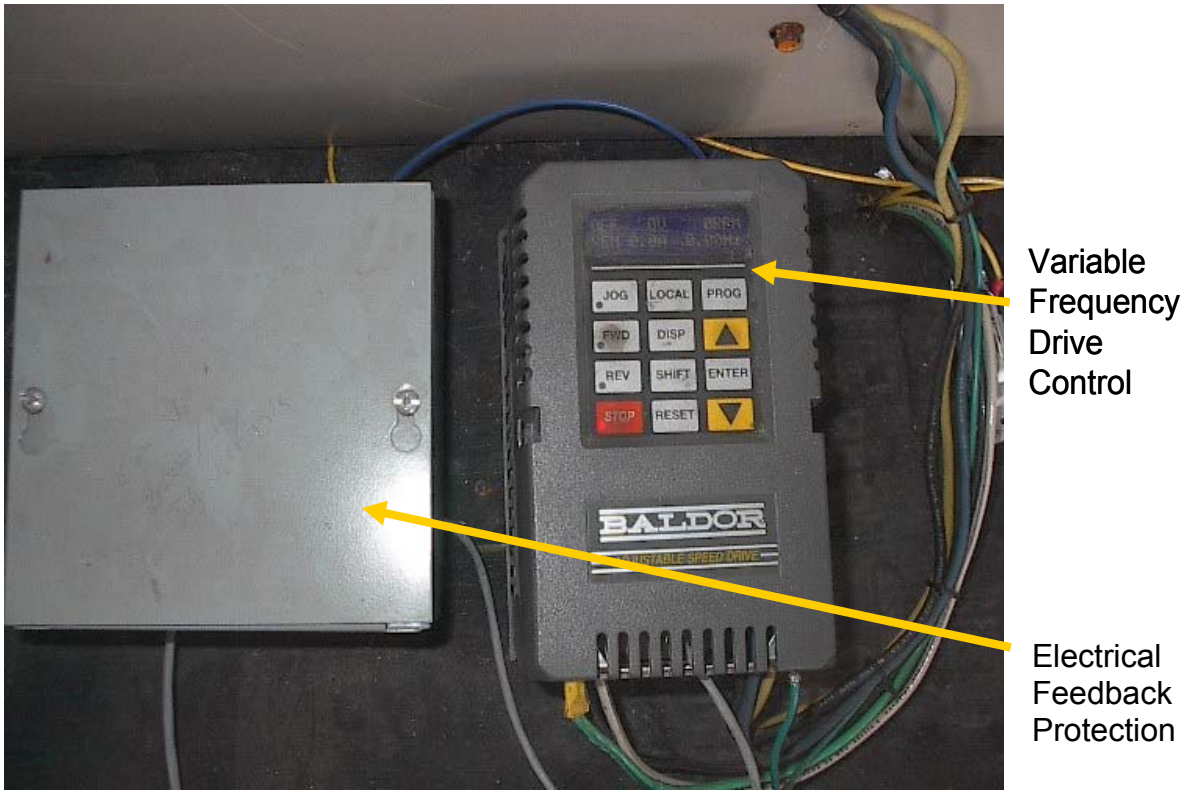

Figure 21. Variable Frequency Drive

2. The user then returned to the Microsoft Excel worksheet entitled "Test Verification Sheet." If the sheet had been closed, the user would re-open it. The tab labeled "FlowCalc" was selected. This sheet contained all the calculations necessary to determine the flow rate of the system based on input variables. The input variable was shown in red text, and their various sources were indicated with comments within the cells. The next set was to begin by completing the variables sourced from the Visual Basic Monitor. These included T1, T2, T3, P1, and ΔP Noz.

	Air Properties		
Inputs	T1 (F)	2.8	65
	T2 (F)	2.83	66
	T3 (F)	2.6	68
	ΔP Noz (inH2O)	0.136	Nozzle Pressure Drop
	Pb (inHg) Internet	30.24	Barometric Pressure
	Twb (F) Winpsych	63	Wet Bulb Temperature
	Pnoz1 (inH2O)	0.171	Static Pressure Before Nozzles
	Tdb (F)	66	Dry Bulb Temperature Average
	Pe (inHg)	0.573	Saturated Vapor Pressure
	Pp (inHg)	0.531	Partial Vapor Pressure
	ρo (lb/ft^3)	0.076	Ambient Air Density
	ρ5 (lb/ft^3)	0.076	In-Station Air Density
	R	53.35	Gas Constant
	α	1.000	Alpha Ratio
	μ (lb/ft*s)	1.226E-05	Dynamic Air Viscosity
	Y	1.000	Expansion Factor
	Re1	2.99E+04	Nozzle 1 Reynolds Number
	Re2	5.98E+04	Nozzle 2 Reynolds Number
	C1	0.963	Nozzle 1 Discharge Coefficient
	C2	0.972	Nozzle 2 Discharge Coefficient
	sumca	0.165	Sum of Coefficients
	CFM(+/-4%)	243	Flow rate thru Nozzle Bank
	Dd. (in.)	6	Duct Diameter (in)
	Ad (ft^2)	0.196	Duct Area (ft^2)
	Vd (ft/s)	1235	Duct Velocity (ft/s)
	Re_{duct}	3.82E+06	Duct Reynolds Number

Figure 22. FlowCalc tab from TVS

3. The user continued completing the FlowCalc sheet by opening Internet Explorer and selecting "Easterwood Weather" from the Favorites list to determine the Barometric Pressure, labeled Pb, in the FlowCalc sheet. The address for the site is: http://www.srh.noaa.gov/ifps/MapClick.php?CityName=College+Station&state=TX&site=HGX.

4. The next step was to open the program entitled "Winpsych." Winpsych is a psychrometric air properties calculation program used to determine the wet bulb temperature given the dry bulb temperature and relative humidity. The values for the dry bulb temperature (labeled Tdb in the FlowCalc sheet) and the relative humidity (read from the Visual Monitor) were then filled in. The check boxes next to each of these were selected and the calculate button was pressed. The resulting wet bulb temperature (Twb) was then displayed. The Test Verifications Sheet was resaved to include these changes.

5. Next, the user began capturing data. The desired CFM was regulated by the presser drop through the flow nozzles, or ΔPnoz. The pressure drop is a function of the output of the VFD. By inputting a value for ΔPnoz, highlighted in yellow, in the FlowCalc the resulting CFM could be determined from the cell labeled CFM, highlighted in green. The fan speed could then be adjusted via the slide bar to raise or lower ΔPnoz. Note: in the event that ambient air testing had desired, steps 6 and 7 would have been omitted.

6. Once the required pressure drop was set, the beige switch at the test stand was flipped to engage the outside compressor unit and cooling coil. Heat could then be added to raise the temperature above that leaving the cooling coil.

7. The user then flipped the Triac control breaker to the "on" position. This breaker is located in the side of the air handling cabinet, and has a yellow power cord entering it as shown in Figure 23. The Triac slide bar was adjusted until the displayed values of T1 and T2 are at 3.0, corresponding to a test dry bulb temperature of 70°F. The system was then allowed to reach steady state; this was indicated by steady pressure drop values, and no difference between T1 and T2.

Figure 23. Triac Control Breaker

8. When the desired flow rate and temperature had been set, data was then able to be captured. First, the data step delay was set in seconds in the monitor window. This is the number of seconds that will elapse between data steps. It was nominally set at one second. The "Export" button was pressed. An Excel sheet was produced, with a new row of data being output at the delay set point. The user pressed the "Save As" button to save the file. After the required numbers of data steps had elapsed, normally fifty, the lower "Stop" button was pressed. This stopped the export of data, and reset the monitor for a new data set. It was observed that the button then returns to reading "Export." The data set was saved using the "Save" command within the produced Excel sheet.

9. Using the FlowCalc sheet, the required ΔPNoz for the next flow point was determined. The VFD slide bar was adjusted to achieve each new flow point, and step 8 was repeated for each desired flow point. At each flow point, the row numbers of the produced Excel sheets would increase by the number of selected data points.

10. The exported data sets were stored in the file labeled "Program." Once all flow point sheets were collected, they needed to be moved to the appropriate "Raw Data" folder within the respective configuration folder. The sets were now ready for reduction and combination.

11. When shutting down the system, it was very important that the correct order be followed. First, zero both the VFD and Triac slide bars. Next, the Triac breaker and cooling coil switch was shut off. Finally, "Stop" was selected on the VFD. At this point, no air should have been moving through the system, and the temperature should be at ambient.

As-Built Test Protocol

In actual as-built examples, duct installation occurs over joists and in hung configurations. To better approximate actual installation conditions, an "as-built" test protocol using two installation configurations was created. The first, termed "board-supported," positioned a duct on top of a continuous flat horizontal board over the entire test length. The second, termed "joist–supported," replicates the duct installation over

1.5” wide supports on 24” center spacing. In this configuration, the duct sags between the joists when compressed and creates a test condition similar to actual installations. The natural sag test configuration occurs when the duct sags between the joists under its own weight, which represents a minimal sag condition. The long-term sag condition was created by increasing the depth of the sag to represent a maximum or “worst-case” condition. Surveys of actual installations by the author were found to be between these configurations.

The tests used non-metallic flexible duct with a single helix core, an R-6 insulation layer, and a foil facing outer layer (vapor barrier). The duct testing used numerous compression ratios to provide a spectrum of data for comparison. These ratios included 0% (maximum stretch), 4%, 15%, 30%, and 45% compression. The compression ratio equals the difference between the compressed length and the maximum stretched length divided by the maximum stretched length. Setting up the compressed duct involved marking the duct in 1’ sections when fully extended and then axially compressing to the desired ratio evenly over the length. Non uniformities in compression increase the total pressure loss with respect to ducts with uniform compression. This approach ensures uniform longitudinal compression over the entire length of the duct under test.

The process for assembling board-supported as-built tests required uniformly compressing the duct supported by a board in a flat configuration. The process for creating the natural sag configuration required removing the board supports and letting the flexible duct sag between the 1.5” wide joists. Since the amount of sag varies

depending upon installation, pressure loss measurements using two extremes of sag were measured. For natural sag, the mid point sag distance ranges from 1" to 3" for duct compressions ranging from 4% to 45%.

Long-term sag was achieved by depressing the duct mid point between the joists and then allowing each section between the joists to retract, emulating a longer term sag condition. Table 2 shows the approximate sag at the midpoint between the supporting joists for the natural and the long-term sag condition, measured from duct centerline to sag centerline. At duct compression below 15%, natural sag and long-term sag are equal since insufficient duct material exists to maintain a greater sag condition. Above 30% duct compression, long-term sag will exceed natural sag as shown in Table 2. Sag creates an increase in the pressure loss through flexible duct and needs to be taken into account in any pressure loss calculation.

	Sag (inches)			
Compression	4%	15%	30%	45%
6" Flex Natural Sag	0.5"	2"	4"	7"
6" Flex Long-Term Sag	0.5"	2"	6"	11.5"
8" Flex Natural Sag	0.5"	2"	3"	4"
8" Flex Long-Term Sag	0.5"	2"	6"	7'
10" Flex Natural Sag	0.5"	1.5"	2"	3.5"
10" Flex Long-Term Sag	0.5"	1.5"	4.5"	6.5"

Table 2. Sag values

The test procedure for joist and board-supported configurations exceeded the requirements in ASHRAE Standard 120-1999 (*ASHRAE 1999*) for all assembly, leak testing and measurements. Measured air property variables include ambient dry bulb

temperature, barometric pressure, chamber dry bulb temperature and relative humidity, and dry bulb temperature at two points within the test duct. Measured pressure loss variables include nozzle plate static pressure, nozzle differential pressure, upstream and downstream static pressure, and test duct differential pressure.

Data Analysis Procedure

Data will be in multiple sets of fifty, stored in the "Raw Data" folder. The resulting pressure drops contained in the individual data sets are not standardized to 100' lengths. This section of the procedure reduced the data into a single sheet, and converted the pressure drop data into ΔP per 100', industry standard. It was important to have the TVS open, as the TVS contains required values for processing.

1. First, all of the individual data sets contained in the new "Raw Data" folder were opened. Additionally, a new sheet was created, and named appropriately. The naming structure was the same as that used on the raw data sets less the flow rate point designation.

2. Within the new sheet two tabs were created, one called "Raw Data" and the other "Reduced." The user began in the first raw data sheet and selected the 1st row containing the row titles, as well as the data points. These selected cells were copied, and pasted into the new sheet in the "Raw Data" tab. The 1st raw data flow point sheet was then closed.

3. The next raw data flow point sheet was opened, and all cells containing data were selected and copied. Each set was pasted below the previous data within the "Raw Data" tab, skipping one row. The raw data flow point sheet was then closed, and the user proceeded to the next flow point. This step was repeated for all of the flow points.

4. Next, one set of fifty rows was selected. In the empty row immediately following the set, the preceding fifty rows were averaged. This formula was extended for the other data columns. This step was then repeated for the other fifty sets of data corresponding to each flow point. The user was left with an

average row for each flow point. Each of these average rows were then copied and pasted into the "Reduced" sheet.

5. Two columns were inserted to the right of the differential pressure column. The first of these two columns was used to input the values to be subtracted for any rigid duct included in the test specimen, and the second was used to output the resulting value for the differential pressure for just the test specimen. The values to be subtracted were input, and the other row was configured to list the resulting value of the net raw differential test pressure. This row was labeled "DP-test."

6. Two other empty columns were inserted to the left of the first column. The first of these columns was used to list the test flow point CFM. The second was used to list the adjusted static pressure loss over 100' labeled "DP-100." The CFM for each flow rate point was inserted into the first column according to its row. In the DP-100 column, the DP-test value was divided by the length of the test section, and then multiplied by 100. This value was the static pressure loss per 100' of test section. The completed "Reduced" tab should have similar column headings to the example Figure 24 below.

CFM	DP-100	P1	DP-.5	Subs	DP-test	P2-.1-t	P7-Noz 1	P5-DP Nozz	P8-Noz 2	T1	T2	T3	Humidity
70	0.417569	0.092	0.080	0.001	0.079	0.012	0.130	0.012	0.117	3.300	3.330	2.833	53.453
80	0.541173	0.119	0.104	0.001	0.103	0.015	0.167	0.015	0.150	3.300	3.330	2.832	53.971
90	0.696169	0.153	0.133	0.001	0.132	0.019	0.211	0.019	0.191	3.299	3.330	2.832	54.112
100	0.852705	0.187	0.163	0.002	0.162	0.023	0.256	0.023	0.233	3.299	3.330	2.831	54.208
110	1.044876	0.229	0.200	0.002	0.198	0.028	0.312	0.028	0.283	3.296	3.328	2.830	54.540
120	1.254605	0.275	0.240	0.002	0.238	0.033	0.371	0.033	0.338	3.295	3.328	2.829	54.556
130	1.497804	0.327	0.287	0.003	0.284	0.038	0.440	0.039	0.401	3.293	3.327	2.828	54.895
140	1.746996	0.381	0.334	0.003	0.332	0.044	0.510	0.045	0.466	3.291	3.326	2.827	55.344
150	2.022223	0.439	0.387	0.003	0.384	0.049	0.586	0.051	0.537	3.288	3.323	2.825	56.005
170	2.696973	0.583	0.516	0.004	0.512	0.062	0.768	0.066	0.702	3.286	3.321	2.824	56.201
180	3.016744	0.650	0.577	0.004	0.573	0.067	0.852	0.073	0.779	3.286	3.321	2.824	56.404
190	3.411112	0.733	0.652	0.005	0.647	0.074	0.956	0.081	0.875	3.287	3.321	2.824	56.676
200	3.900223	0.840	0.746	0.005	0.740	0.083	1.086	0.092	0.092	3.288	3.323	2.824	56.648

Figure 24. Example "Reduced" tab column headings

7. The data was now reduced, and put in terms of 100' lengths. It was now able to be plotted and displayed as desired.

CHAPTER VIII

EXPERIMENTAL RESULTS

The resulting data displays static pressure drop as a function of volumetric flow rate for each of the three sizes of non-metallic flexible duct: 6", 8", and 10" duct. In each of the plots, the static pressure drop through rigid sheet metal duct of the same diameter is presented as a comparative baseline for the results. Straight run compression configurations that were tested include rigid sheet metal duct, maximum stretch flexible duct, 4% compressed flexible duct, 15% compressed flexible duct, 30% compressed flexible duct, and 45% compressed flexible duct. Each compression configuration contains data for both board and joist-supported configurations as considerable differences exist between the two. Compression ratios higher than 15% also include short and long-term sag configurations to provide a range of values. Accuracy compared to published reference was ±4%.

Straight Run Compression Configurations

Results are presented first by size and second by compression ratio. The included size graphs allow direct comparison of various compression ratios ranging between maximum stretch and 45% compression in the same duct size. The compression ratio plots allow comparison of all three duct sizes, 6", 8", and 10", for a given compression ratio. In this manner, trends relating to size and to compression ratio may be observed.

Rigid sheet metal duct was tested for each size for agreement with existing ASHRAE/ACCA numbers (ASHRAE Handbook-Fundamentals 2005 Chapter 35-Duct Design). The rigid duct was tested under the same volumetric flow rate range as the flexible duct. Resulting values for the rigid duct showed agreement to within ±5% of ASHRAE values. The rigid sheet metal duct serves as a comparative baseline. Maximum stretch flexible duct displayed losses within ±2% of rigid duct losses for all three duct sizes under test. Due to this result, maximum stretch flexible duct may be considered a baseline for static pressure loss comparison as well.

6" Duct Results

The first and smallest duct size tested was a 6" duct. The 6" duct was tested over a flow range of 70 CFM to 170 CFM. These flow ranges, and the flow ranges of the other duct sizes tested, were determined after communications with industry suppliers and manufacturers. No data was taken below this flow range even though 6" duct is used occasionally to transport flow rates less than 70 CFM. This is due to the fact that the experimental test setup cannot produce flow rates lower than 70 CFM while maintaining flow accuracy and stability levels less than 5% and greater than 95%, respectively.

The results for straight run compression testing on 6" duct may be viewed in Figure 25. Analysis of the resulting data reveals that static pressure losses increase as compression increases and/or flow rate increases. At 70 CFM the increase in magnitude of static pressure loss from maximum stretch to 45% compressed long-term joist supported was 46 times. At 150 CFM, the increase in magnitude for the same

configurations was 52 times. The static pressure loss in inH_2O per 100' for 45% compressed long-term joist supported flexible duct at 70 CFM was 1.86 inH_2O. The blowers used in 5-ton rated residential units will typically produce an operating static pressure of approximately 1.0 inH_2O. This indicates that a room designed to receive 70 CFM, connected to the unit with 45% compressed long-term sag joist-supported flexible duct, would not receive full airflow as the static pressure loss through the duct is greater than the operating produced static pressure of the blower.

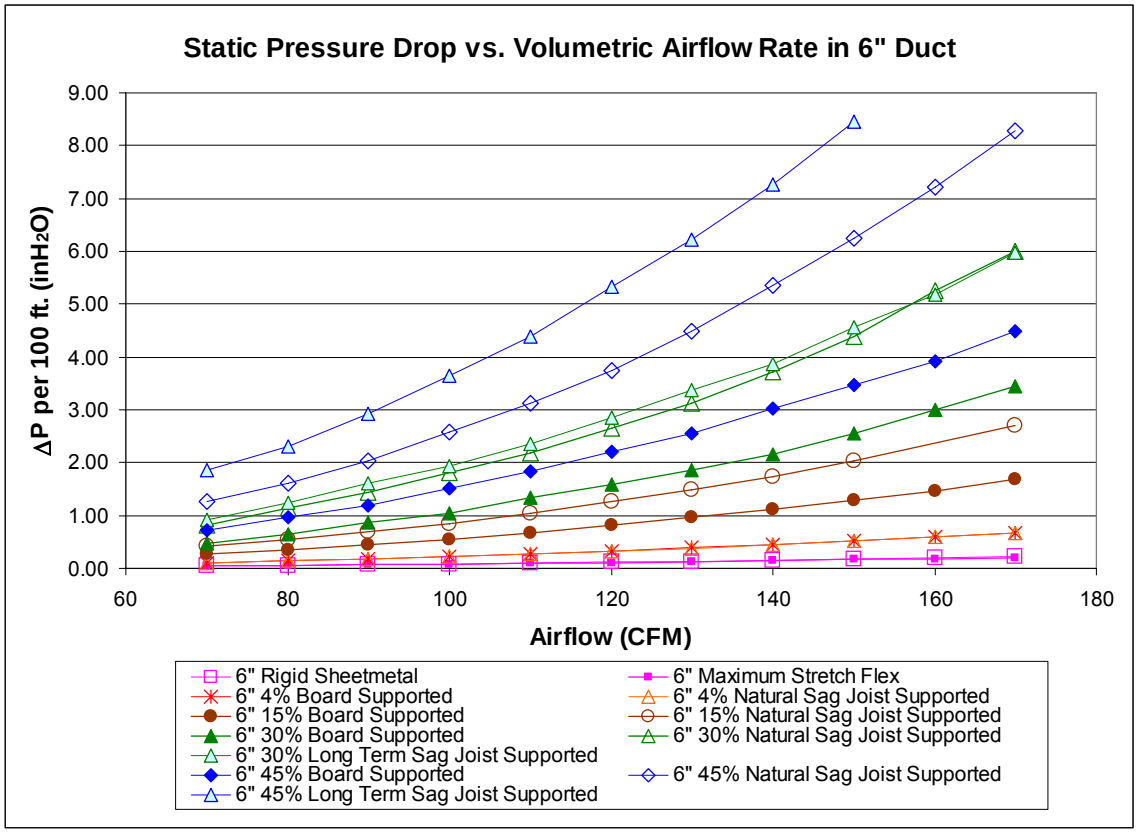

Figure 25. Results for 6" duct

8” Duct Results

The testing of 8” duct occurred at a flow range of 140 to 260 CFM. Static pressure loss for 8” maximum stretch flexible duct at 140 CFM was 0.039 inH_2O; while static pressure loss for 45% compressed long-term sag joist-supported flexible duct was 1.56 inH_2O at 200 CFM. This is an increase in magnitude of 39 times. At 220 CFM the same configurations showed a magnitude increase of 45 times. 8” flexible duct again displayed an increase in static pressure drop as both compression and flow rate increased. Results for 8” duct may be viewed in Figure 26.

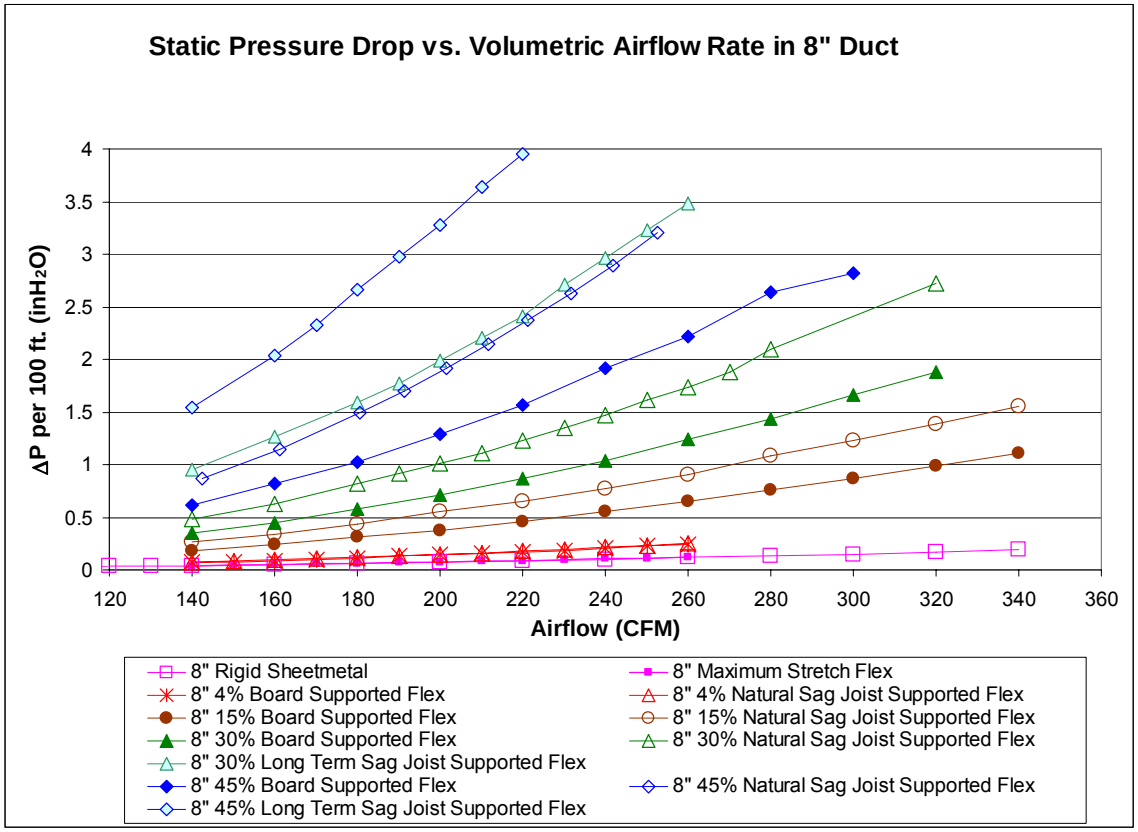

Figure 26. Results for 8” duct

10” Duct Results

The testing of 10” duct occurred at a flow range of 200 to 400 CFM. Static pressure loss for 10” maximum stretch flexible duct at 200 CFM was 0.024 inH_2O; while static pressure loss for 45% compressed long-term sag joist-supported flexible duct was 1.139 inH_2O at 200 CFM. This is an increase in magnitude of 47 times. At 340 CFM, the same configurations showed a magnitude increase of 51 times. 10” flexible duct again displayed an increase in static pressure drop as both compression and flow rate increased. Results for 10” duct may be viewed in Figure 27.

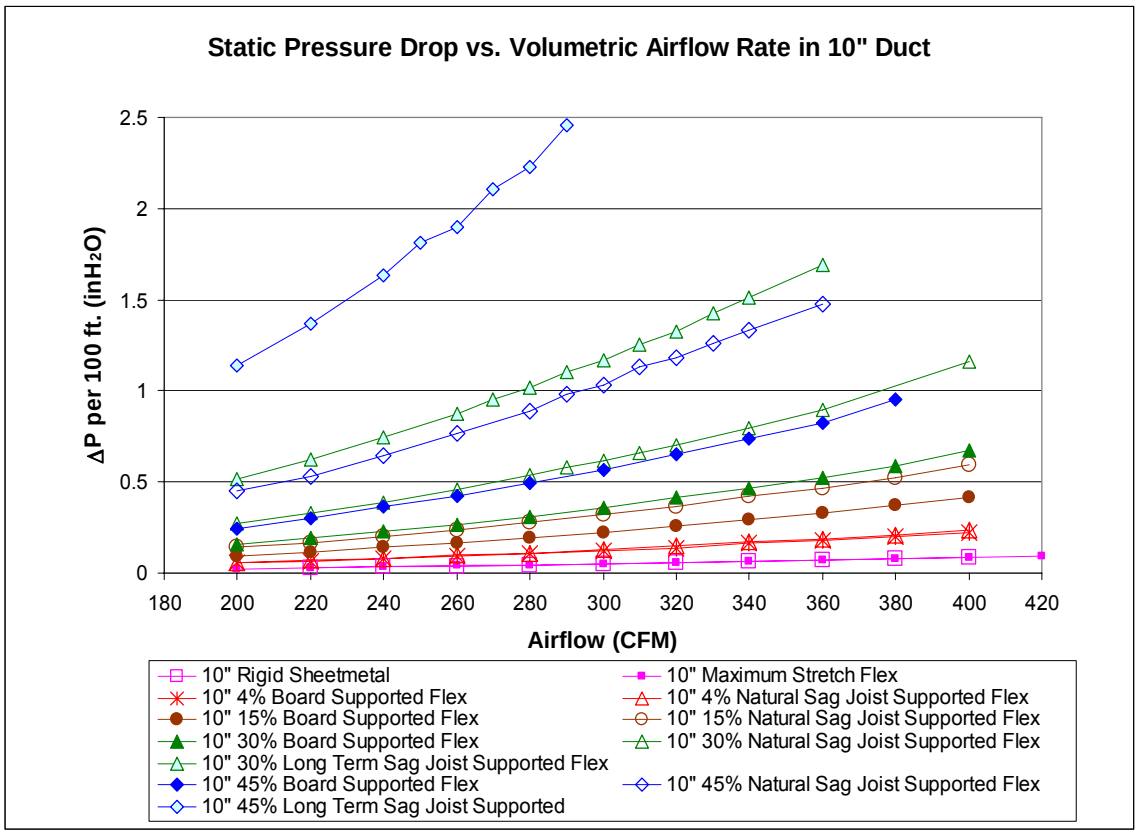

Figure 27. Results for 10” duct

Maximum Stretch Configuration

Results comparing the static pressure loss through maximum stretch flexible duct with static pressure loss through rigid duct showed agreement within 2%. For comparative purposes, rigid sheet metal duct was tested utilizing both 3' and 5' standard commercially available section lengths in the 6" size. This comparative testing allows the individual contributions of transition and length to be ascertained. The resulting data showed that section length has less than a 5% effect on the static pressure drop over the measured flow range. Results for maximum stretch configuration may be viewed in Figure 28.

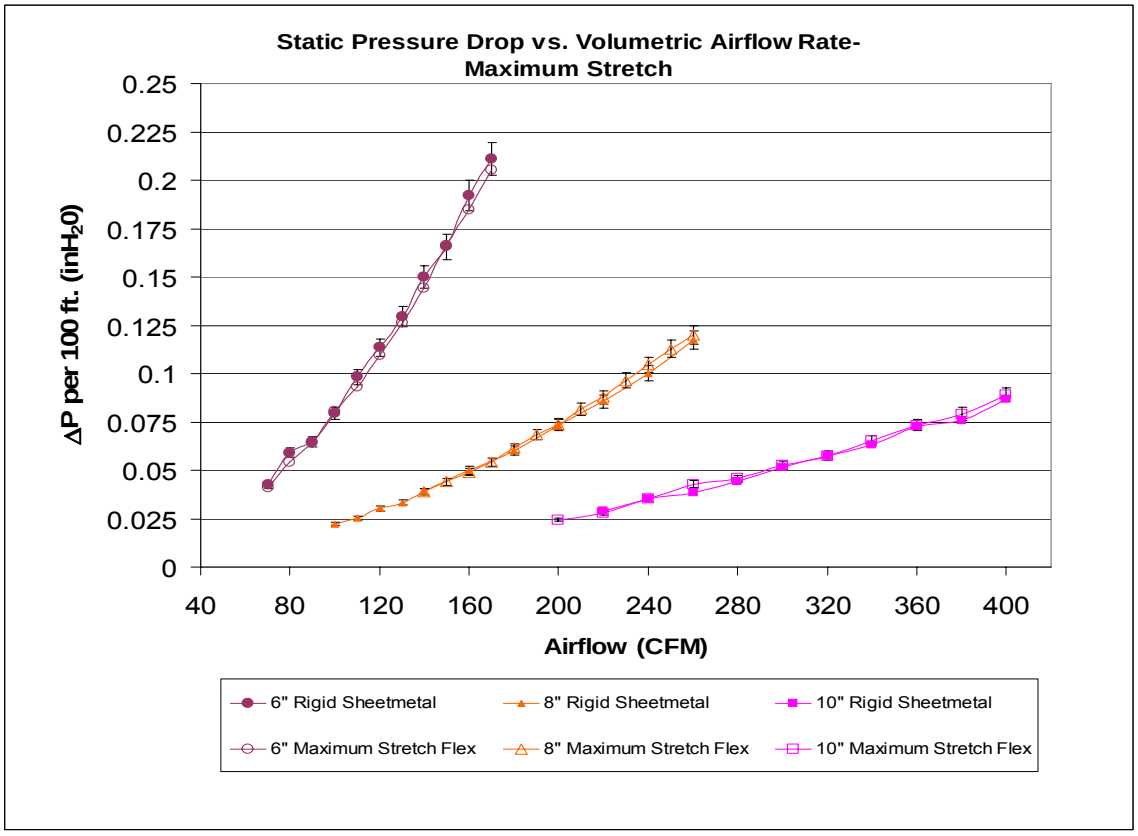

Figure 28. Maximum stretch configuration results

4% Compression Configurations

4% compression revealed increases in static pressure drop when compared to maximum stretch results. A 4% compression rate results in 1' of compression for a 25' length, resulting in 25' of flexible duct occupying a length of 24'. The duct weight caused the natural sag to occur when the supporting boards were removed at the completion of the board supported tests (flat configuration). At 4% compression, less than 1" of sag below the duct supports occurred. The data from the ASHRAE Handbook, adjusted with ASHRAE correction factors, agrees with the 4% compression data taken to within ±20%. Results for 4% compression duct may be viewed in Figure 29.

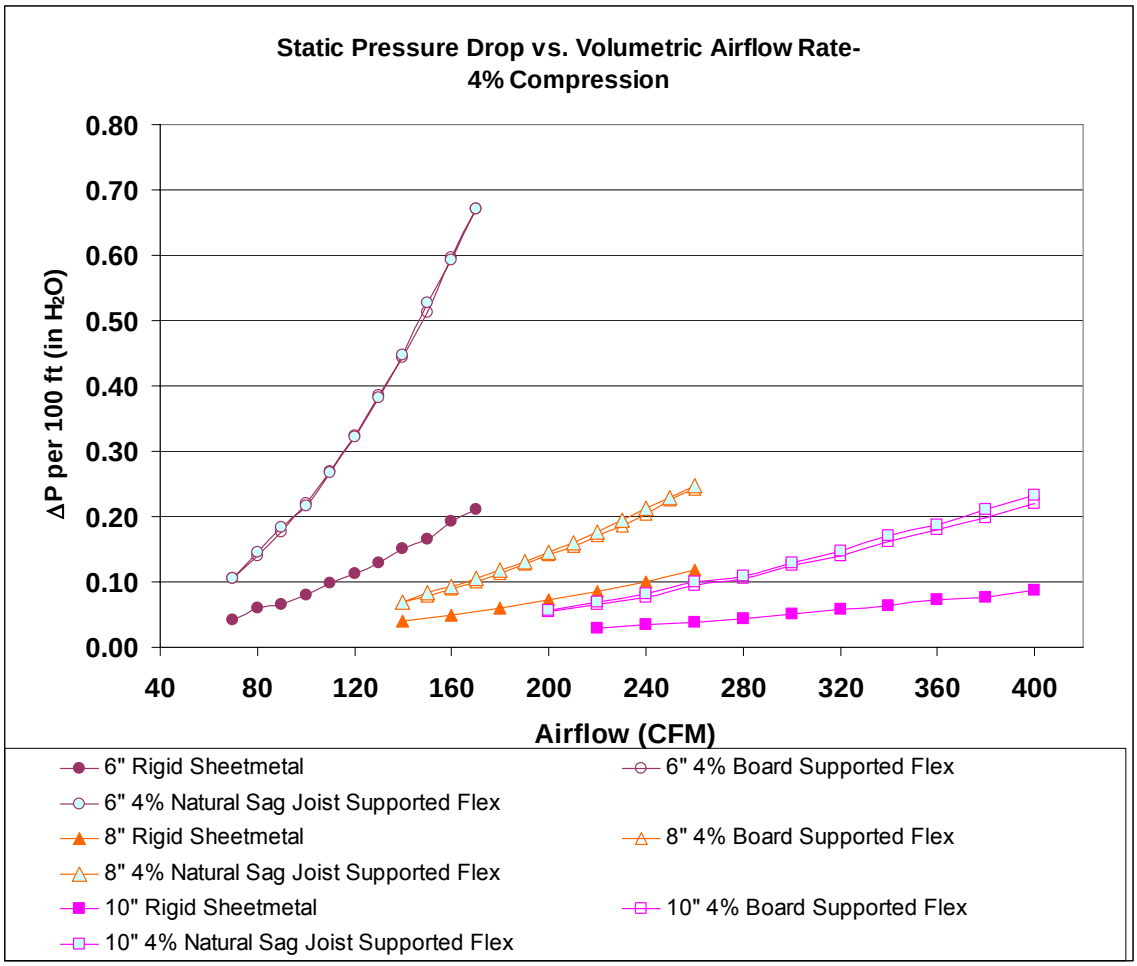

Figure 29. 4% Compression configuration results

15% Compression Configurations

The 15% compression values were found to be sensitive to the uniformity of compression and variations from these values should be expected in field installations. Results for 15% compression duct may be viewed in Figure 30.

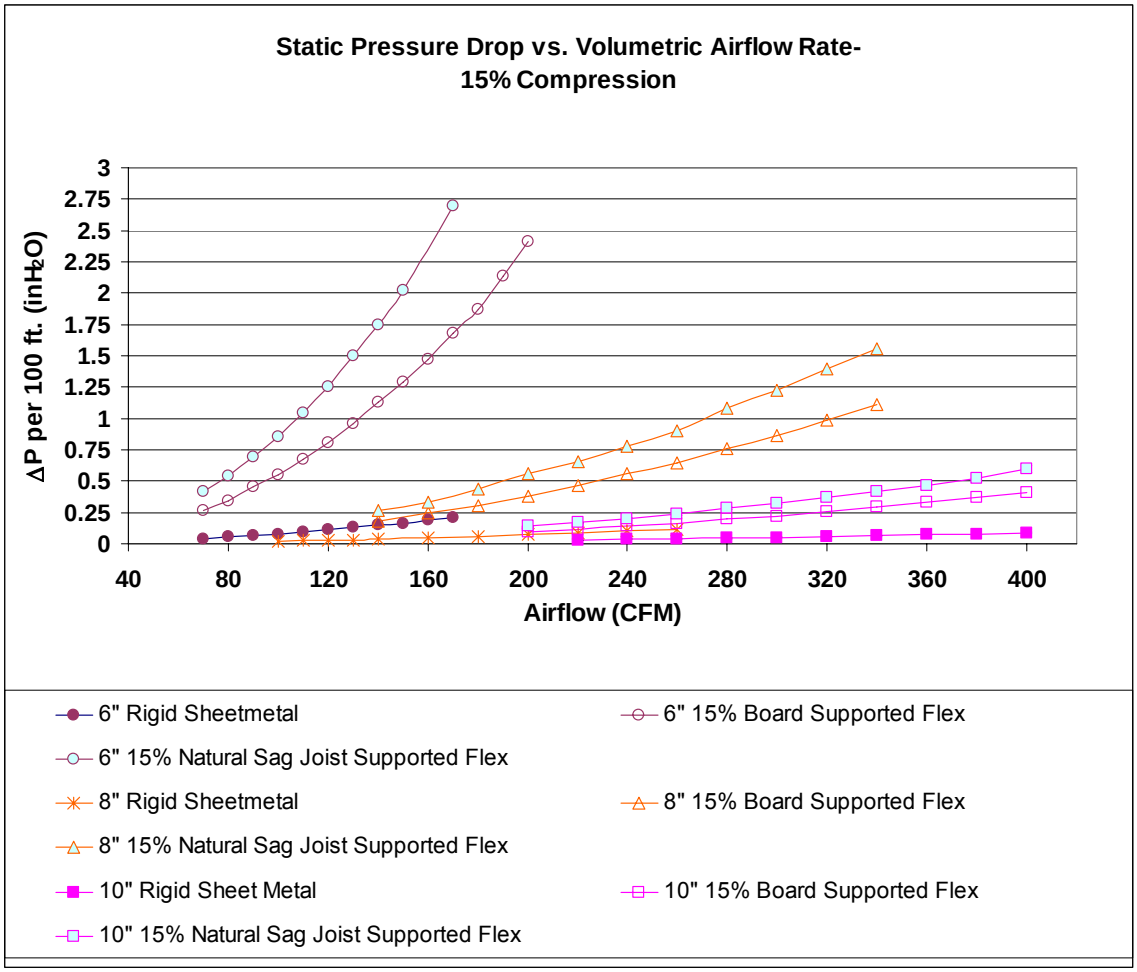

Figure 30. 15% Compression configuration results

30% Compression Configurations

The 30% compression results continued to demonstrate a high sensitivity to uniformity and degree of compression. Results for 20% compression duct may be viewed in Figure 31.

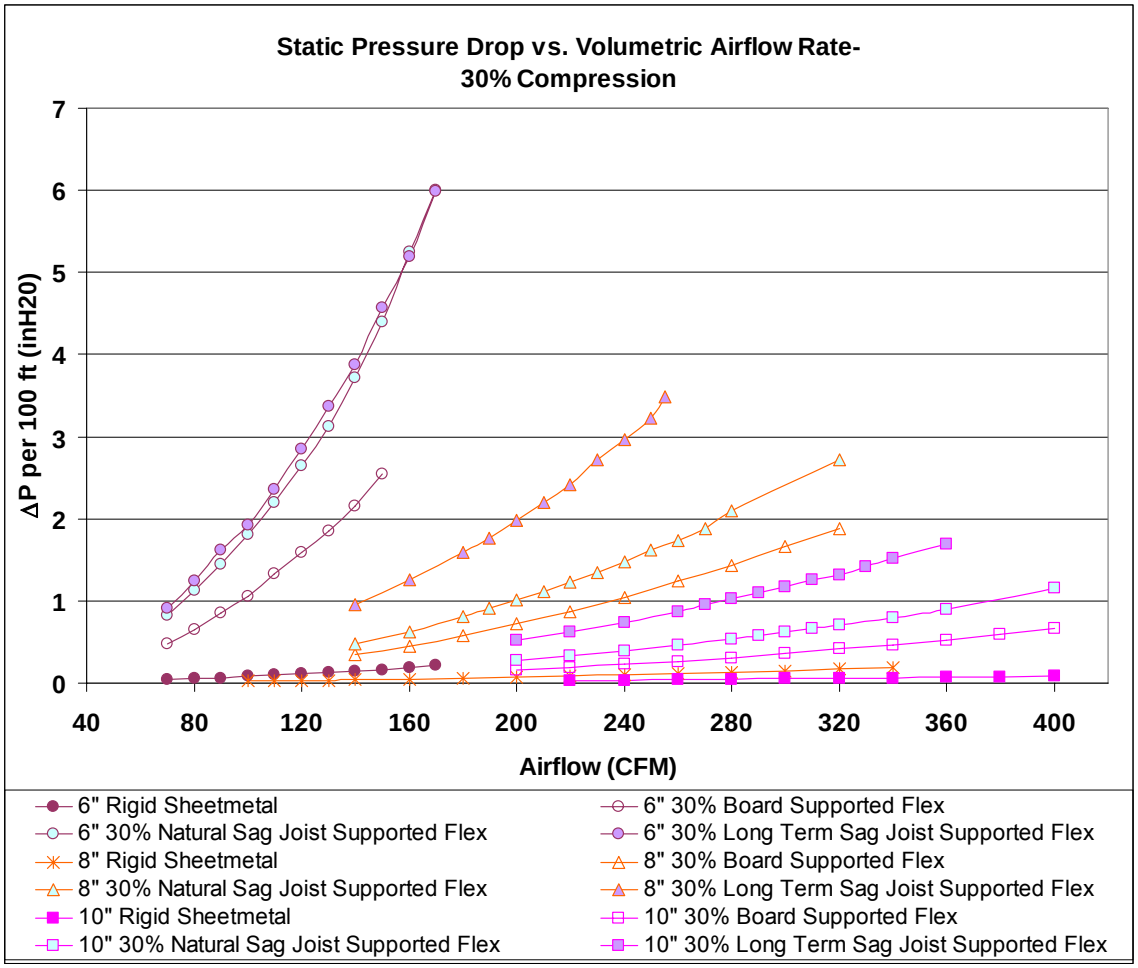

Figure 31. 30% Compression configuration results

45% Compression Configurations

The 45% compression results are displayed in Figure 32. Measured losses climbed to over 8 inH_2O for 6" duct, 4 inH_2O for 8" duct, and over 3 inH_2O for 10" duct.

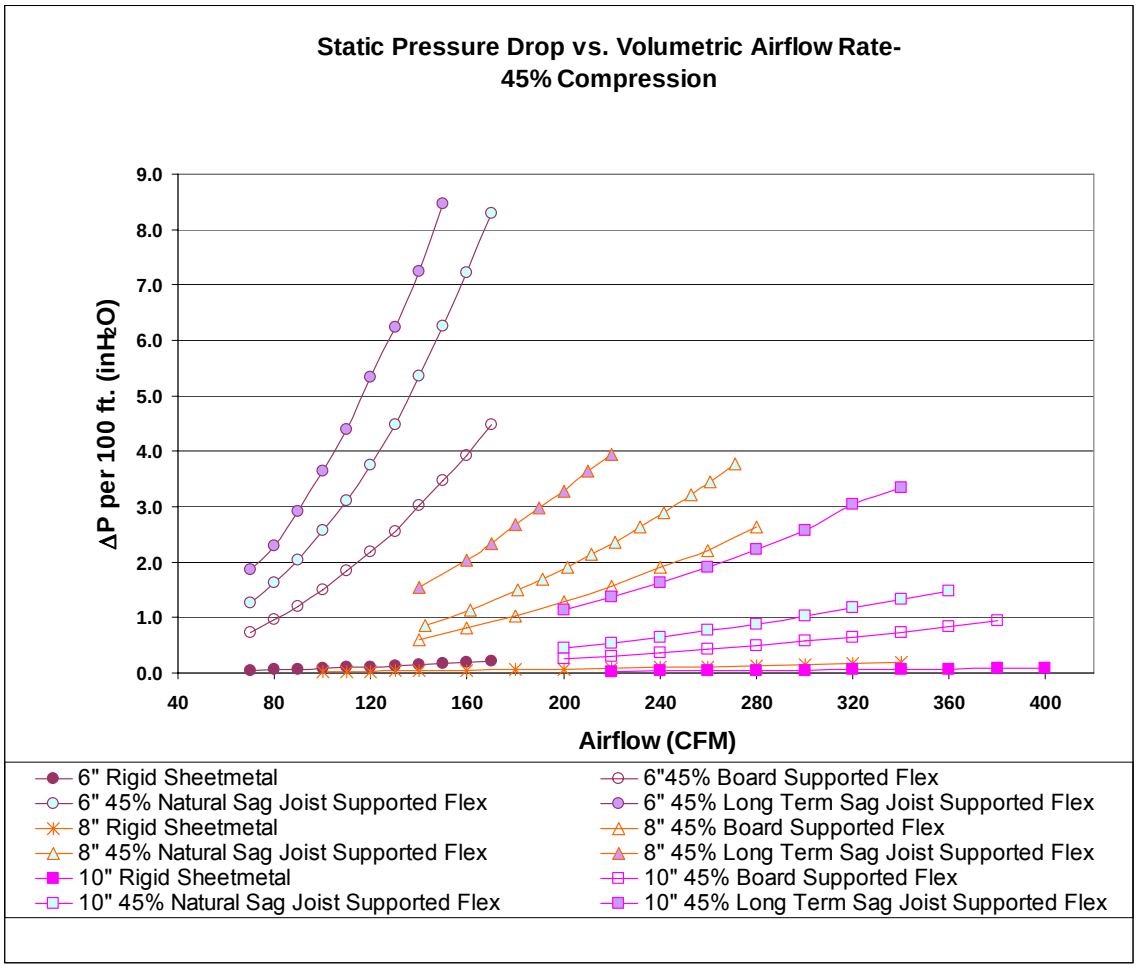

Figure 32. 45% Compression configuration results

CHAPTER IX

ERROR ANALYSIS

Experimental error may be caused by several sources: sensor inaccuracy, potential leakage, random error, non-uniform compression, variances in duct manufacture, and others. Measures were taken in the design and construction of the test setup, and in the experimental procedure, to reduce error as much as possible.

To minimize sensor accuracy all sensors used within the test setup have an accuracy of 2% full scale or better, displayed in Table 3. Sensors were calibrated with NIST-traceable certificates and then re-calibrated using NIST-certified devices as the experiment progressed. Error from leakage was minimized by testing for total system leakage prior to data collection, as detailed previously in Chapter XII-Experimental Procedure.

In order to minimize the influence of random experimental error, the DAQ acquires 5,000 individual readings for each point of data. This occurs by taking 100 readings each second and calculating the average of those 100 readings. This process then repeats 50 times with each point value stored on disk. These 50 data sets are then averaged to provide one set of values for each data point.

Another source of error when testing compressed flexible duct is with regard to the non-uniformity of compression within the duct. Although steps were taken to ensure equal spacing and uniform compression of the insulator, there is no way to determine uniform compression of the single-helix duct liner. This non-uniformity will cause some

variation in repeatability. Variances in actual final product between different manufacturers also attribute to final error.

Pressure loss values for metal duct are well documented within the ASHRAE Handbook-Fundamentals (ASHRAE 2005). Therefore, pressure loss results of the test setup were compared to published figures. For all sizes and flow rates error was found to be less than ±4%. This provides a high level of confidence as to the test results for non-metallic flexible duct.

An analysis of sensor accuracy yields the following maximum errors for each measurement:

Sensor	Manfr.	Model	Element	Range	Unit	% Accuracy (+/-FS)	Drift	Output	Response Time (mS)
Δ Pressure	Dwyer	607-0	Silicon Diaphram	0:.1	inH_2O	0.25%	.5% FS/yr	4:20 mA DC	250
Δ Pressure	Dwyer	607-1	Silicon Diaphram	0:.25	inH_2O	0.25%	.5% FS/yr	4:20 mA DC	250
Δ Pressure	Dwyer	607-21	Silicon Diaphram	0:.5	inH_2O	0.50%	.5% FS/yr	4:20 mA DC	250
Δ Pressure	Dwyer	607-3	Silicon Diaphram	0:1	inH_2O	0.50%	.5% FS/yr	4:20 mA DC	250
Δ Pressure	Dwyer	607-4	Silicon Diaphram	0:2	inH_2O	0.50%	.5% FS/yr	4:20 mA DC	250
Temperature	Dwyer	650-2	Silicon Junction	20:120	°F	0.30%	.5% FS/yr	4:20 mA DC	500
				Humiditiy: 0:90%		2%			
				Humidity: 90:99%	%RH	2%+1%M			
Temp/RH	Vaisala	HMD60Y	Humidcap/Platinum	Temperature:20:80	°C	.6 °C		0:10 V	15000

Table 3. Sensor specifications

Inputs (IP) [SI]

The input variables are measurable, either from the test system or visually, then used in the calculations that follow.

ΔP_{noz} Measured static pressure drop through nozzle bank. Captured using monitor program. (inH_2O) [Pa]
Sensor Accuracy: .25% FS
Sensor Error: ±0.000625 inH_2O

T_{db} Dry bulb temperature of air within test duct. Recorded from T_1 and T_2. (°F) [°C]

Sensor Accuracy: .5% FS
Sensor Error: ±.36°F

Pb Barometric pressure. Recorded from barometric pressure sensor within laboratory, or collected from weather data for Easterwood Airport, which is located eight miles from the test location. (in-Hg) [kPa]
Sensor Accuracy: Remote
Sensor Error: Assume 1 in-Hg

T_{wb} Wet bulb temperature of air within test system. Calculated using psychrometric properties for air with inputs of dry bulb temperature (T_{db}) and relative humidity (RH) from monitor program. (°F) [°C]
Sensor Accuracy: Calculated Combined Error of 2% FS
Sensor Error: 1.6 °F

T_{amb} Ambient temperature within laboratory at time of test (°F) [°C]
Sensor Accuracy: .3% FS
Sensor Error: ±.36°F

P_{noz1} Static pressure in inH_2O recorded before nozzle bank with monitor program (inH_2O) [pa]
Sensor Accuracy: .5% FS
Sensor Error: ±.0025 inH_2O

By applying potential sensor accuracy error to each input variable, total possible percentage error can be calculated via the *Test Verification Sheet* mentioned previously. For overall testing temperature range, maximum calculated error never exceeded ±1.6%. The largest measured pressure loss for any test configuration was 8.56 inH_2O. The calculated error for this measurement would then be 0.136 inH_2O.

These results suggest that the sensor error of the test apparatus is of minor influence when determining total error. Total error and repeatability are influenced much more from the individual test configuration being tested. This includes variations in the morphology of the internal duct liner and variation in manufacturing tolerances between various duct producers. From testing experience variation in inner liner

morphology seems to have the largest influence in impacting test repeatability. This conclusion is consistent when comparing calculated test apparatus error of ±1.6% to calculated % error vs. published sources of ±4%. Plots below display the appropriate amount of applied error in the form of ± error bars.

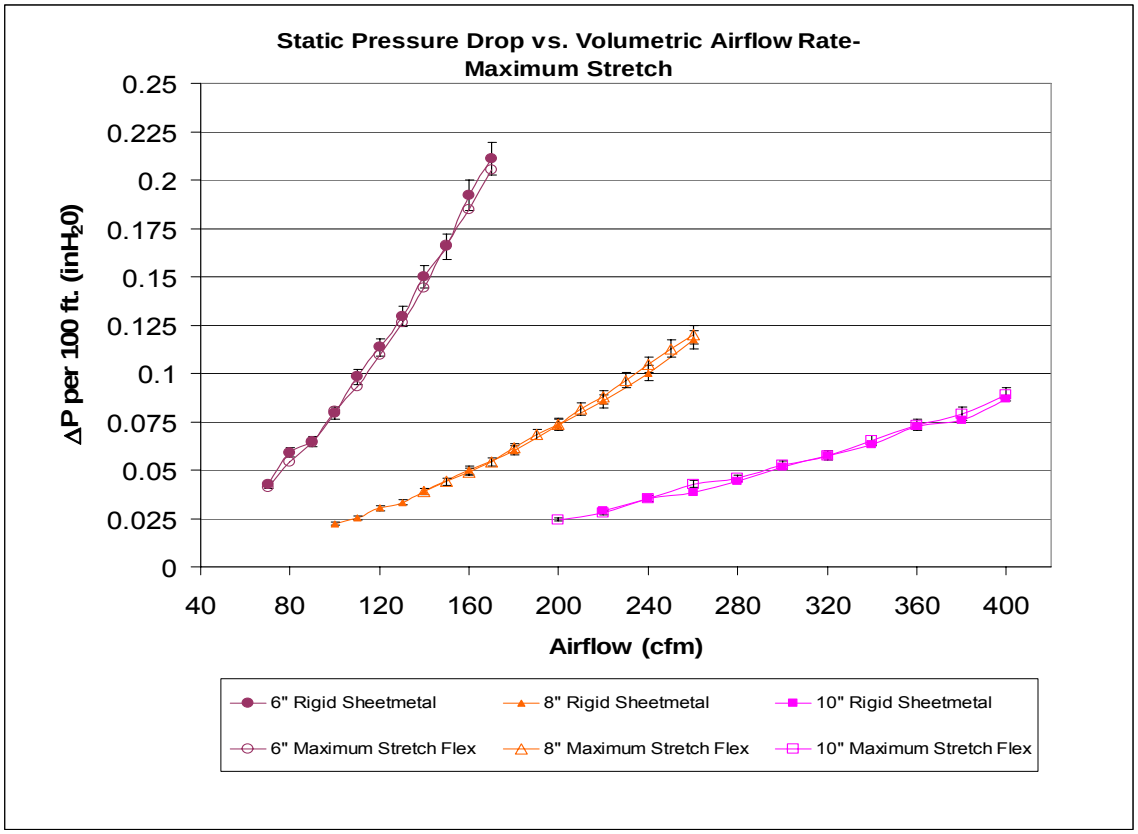

Figure 33. Error analysis-maximum stretch configuration

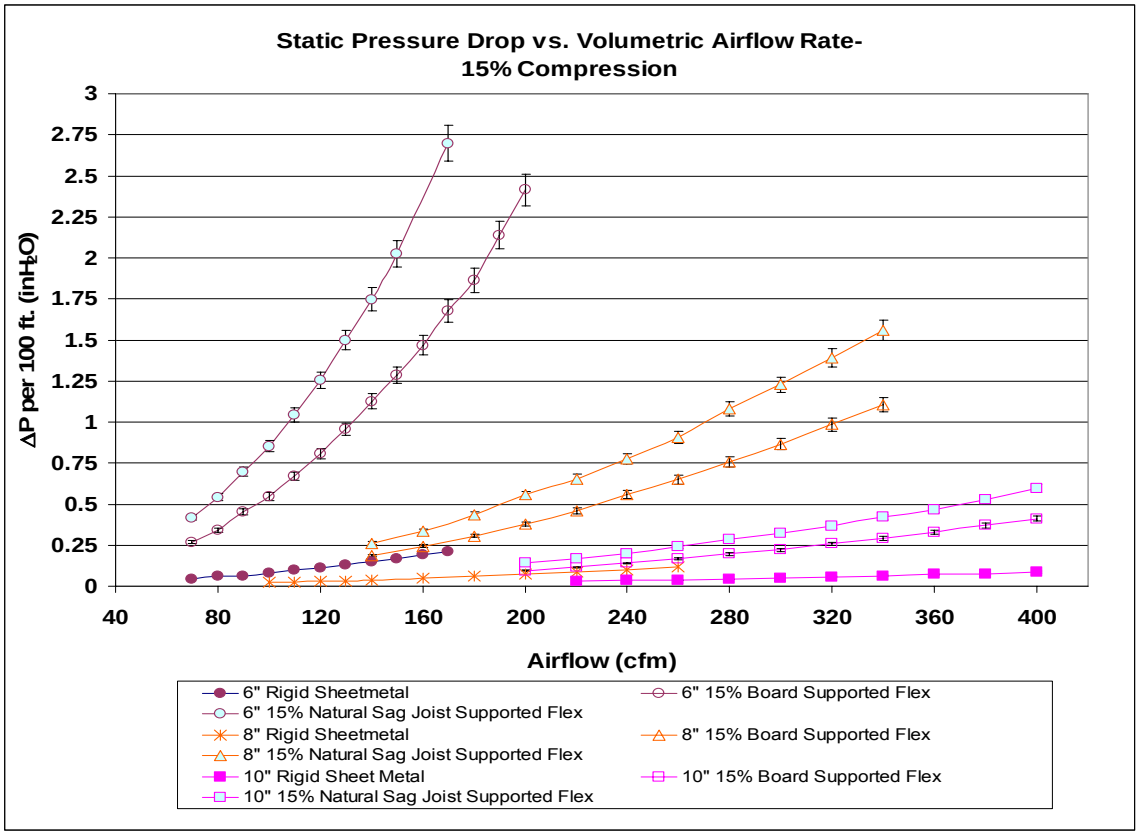

Figure 34. Error analysis-15% compression configuration

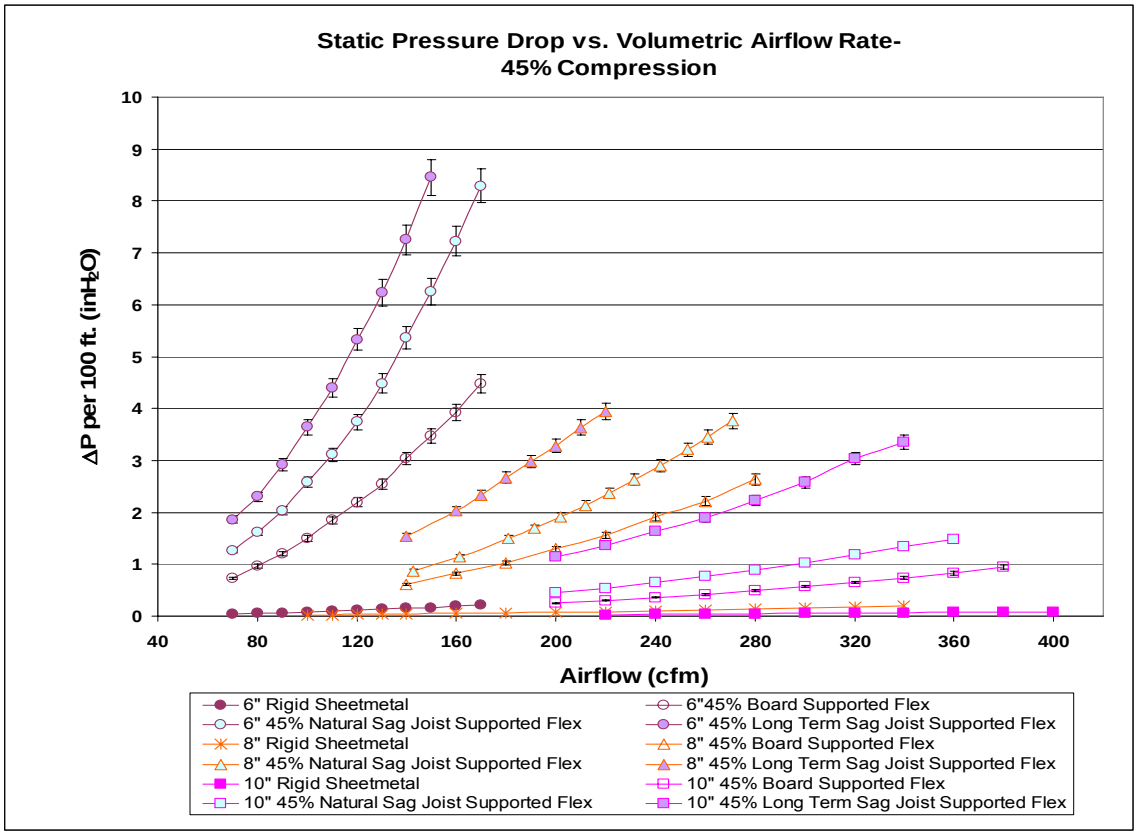

Figure 35. Error analysis-45% compression configuration

CHAPTER X

DEVELOPMENT OF LOSS PREDICTION EQUATIONS

The current methodology to determine the pressure loss through flexible duct involves estimating the amount of compression (L / L_{FE} – see the 2005 ASHRAE Handbook Fundamentals, page 35.7, Figure 8) and then applying the correction factors for the specified flexible duct. This method only considers straight flexible duct. This section details an approach which extends the calculations to calculate the pressure loss over a range of compression with natural sag and long-term sag exhibited by ducts installed over joists on 24" centers.

Currently, no equation exists which incorporates compression as a variable and which may be universally applied to flexible duct. The existing method applies ASHRAE correction factors to rigid duct data. Static pressure loss for ductwork normally uses the Power Law to express pressure loss in units of inH_2O per 100 feet. This equation contains a coefficient of C, the flow rate in CFM, and some exponent, n. The value of "n" is normally assumed to be two, although it fluctuates in actual applications.

In order to create a method for predicting the static pressure loss in flexible duct, the necessary input variables and constraints had to first be determined. Input variables include duct diameter (D_d, in.), flow rate (CFM), percent compression ($C_{,\%} = ((1-L)/L_{fe})$), and the amount of sag in joist-supported configurations. Constraints included standard temperature and pressure, as well as uniform compression throughout the duct

length, which requires that each linear section of the duct be compressed equally compared with the other sections of the duct.

A set of predictive coefficients for the coefficient "C" used in the Power Law was created based on experimentally determined data. Using these coefficients, plots and tables were created which allow for the prediction of static pressure loss (inH_2O per 100') for various configurations and flow rates. The new coefficients correct the static pressure loss produced from the Power Law by adjusting the coefficient of 'C' to compensate for the difference in the exponent from the traditionally assumed value of two. These are based on assumed nominal flow rates to provide minimum error compared to the actual data. The nominal flow rates used are 100 CFM for 6" duct, 150 CFM for 8" duct, and 250 CFM for 10" duct. The exponent, n, used in the predictive equation is always two. The % error is less than ±7% for every case within the range of ±30 CFM of the nominal CFM. The calculated static pressure losses produced using the corrective coefficients were also compared to actual losses for flow rates outside the nominal CFM by more than 100%. In every case the resulting % error was less than 15%. The Power Law equation (Eqn. 10.1) is:

$$\Delta P(in - H_2 0\ per\ 100 ft.) = C * cfm^n \quad \textbf{(10.1)}$$

Using the predictive coefficient of Ce (C-estimated) and a value of two for the exponent (Eqn. 10.2), the predictive Power Law becomes:

$$\Delta P(in - H_2 0\ per\ 100\ ft.) = Ce * cfm^2 \quad \textbf{(10.2)}$$

With the corrective coefficients, the static pressure loss could now be accurately predicted for 6", 8" and 10" duct with compression ranging from fully stretched to 45% compression. Three configurations, including board-supported (flat), natural sag, and long-term sag, were chosen. The applicable corrective coefficient can be sourced from the table and then input into the Power Law along with CFM and the exponent of two. This set of three equations provides the static pressure loss prediction for any compression ratio with an accuracy of ±10%.

Figure 36 shows the range of data obtained for the coefficient of C, with the three configurations using 10" flexible duct. This shows the impact of sag in determining and predicting the pressure loss under different conditions.

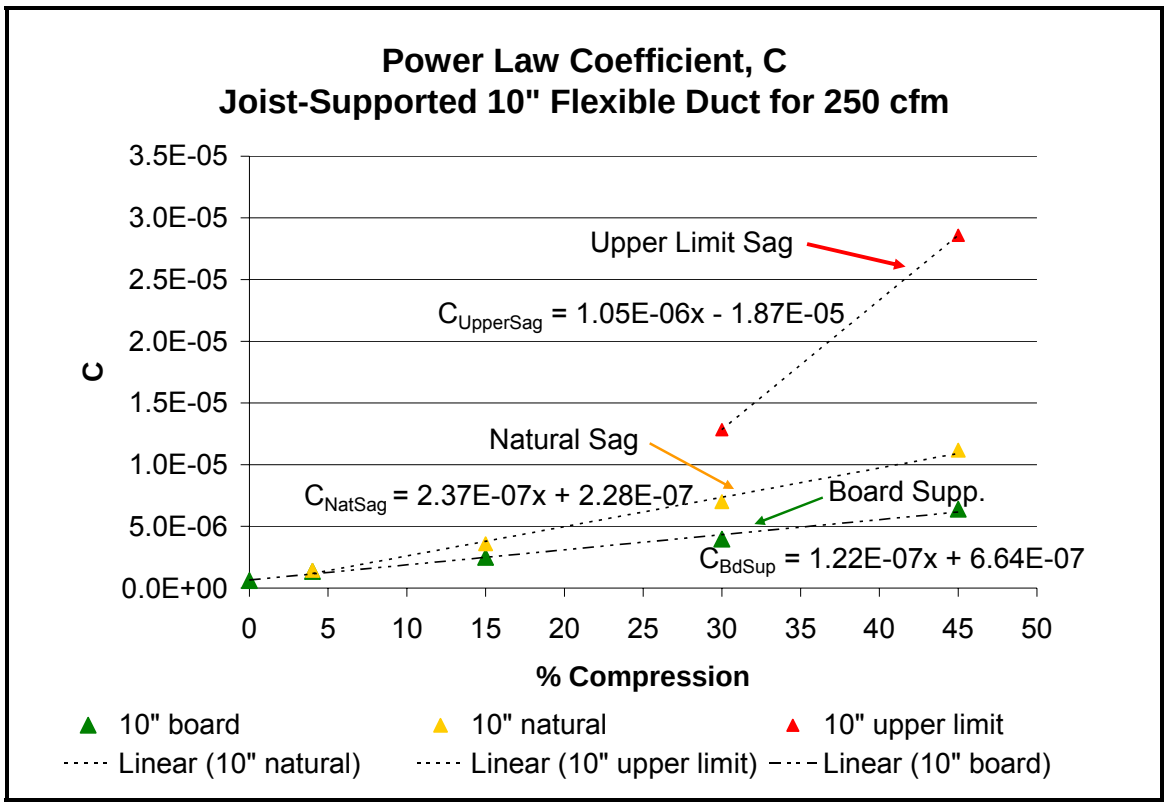

Figure 36. Example plot displaying equation of the line for each configuration

Using the extracted line equations to solve for Ce, at any percent compression, a new set of plots (Figure 37) were created that display duct size on the x-axis and Ce on the y-axis. Using this data, an equation was derived for each of the three configurations: one for board-supported configurations (Eqn. 10.3), one for natural sag configurations (Eqn. 10.4), and one for long-term sag configurations (Eqn. 10.5).

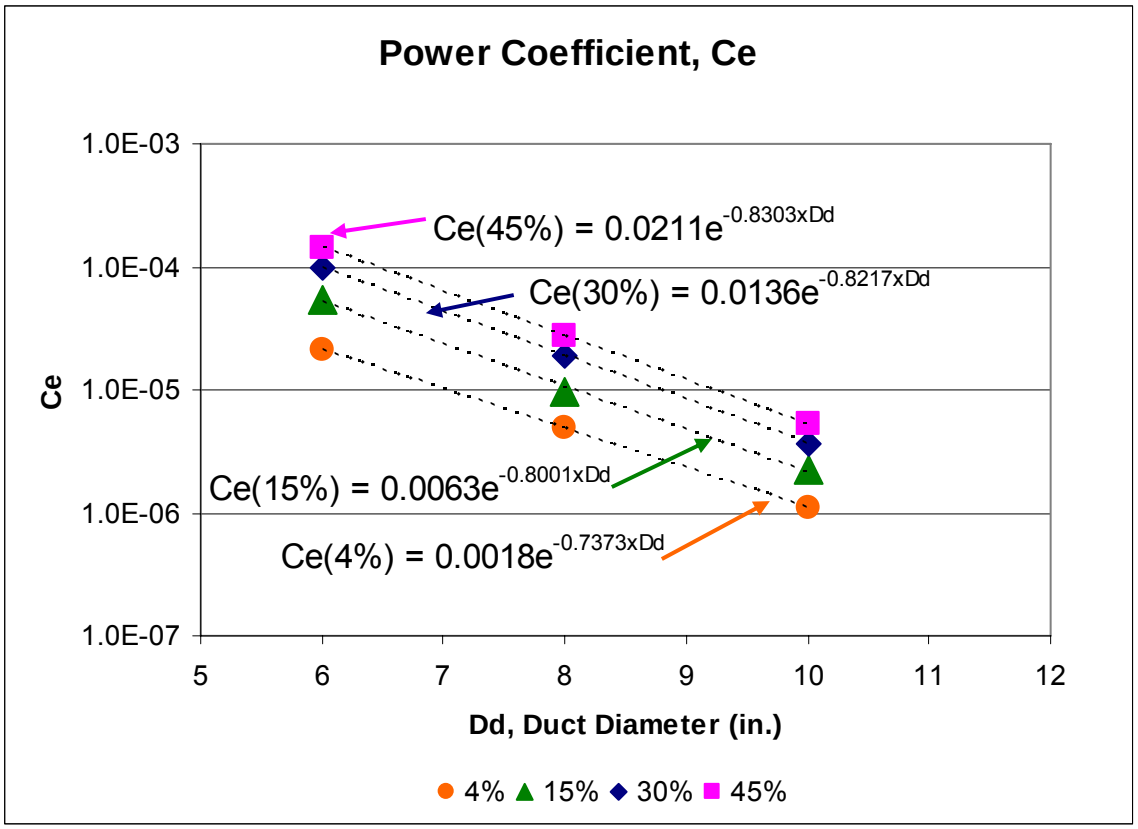

Figure 37. Corrective coefficient given duct size and percent compression

A range of static pressure loss values may now be predicted for any duct configuration. The minimum value is associated with the board-supported equation. The maximum value is associated with either the natural sag equation or the long-term sag configuration, depending on percent compression. The natural sag equation can be used for percent compression under 15%, and the long-term sag equation should be used for all percent compression configurations over 15%.

Board-supported

$$C_{e,b} = (5\times10^{-4} * C_{\%} - 4\times10^{-4})\ e^{(-.0392LN(C_{\%})-.6866)*D_d} \quad \textbf{(10.3)}$$

Natural Sag

$$C_{e,n} = (9\times10^{-4} * C_{\%} - 1.9\times10^{-3})\ e^{(-.0297LN(C_{\%})-.7368)*D_d} \quad \textbf{(10.4)}$$

Long-term Sag

$$C_{e,l} = (4\times10^{-5} * C_{\%} + .016)\ e^{(-.74*D_d)} \quad \textbf{(10.5)}$$

Example

Equation 10.6 shows the pressure loss per 100' for 15% compressed board-supported 6" flexible duct flowing 100 CFM using actual measured data, complete with the actual extracted coefficient of C and value of n:

$$\Delta P(inH_2 0\ per\ 100\ ft.) = 3.705\times10^{-5}\times100^{2.09} = .561\ inH_2O \quad \textbf{(10.6)}$$

Equations 10.7 through 10.11 show the calculated pressure loss per 100' in 15% compressed 6" flexible duct flowing 100 CFM using empirically determined and corrected coefficient of Ce (calculated) with a standard value of 2 for n:

$$C_e = (5\times10^{-4} * C_{\%} - 4\times10^{-4})e^{(-.0392LN(C_{\%})-.6866)*D_d} \quad \textbf{(10.7)}$$

$$C_e = (5\times10^{-4} * 15 - 4\times10^{-4})e^{(-.0392LN(15)-.6866)*6} \quad \textbf{(10.8)}$$

$$C_e = 6.103\times10^{-5} \quad \textbf{(10.9)}$$

$$\Delta P\ per\ 100\ ft. = C_e * cfm^2 \quad \textbf{(10.10)}$$

$$\Delta P\ per\ 100\ ft. = 6.103\times10^{-5} * 100^2 = 0.61\ inH_2O \quad \textbf{(10.11)}$$

The predictive approach yields a percentage error of 8.7% compared with the actual value of 0.561 inH_2O. For a joist-supported duct, this value represents the minimum static pressure loss. The maximum static pressure loss could be calculated in the same manner and using the equation for natural sag configurations. Using this method, a predictive range of loss for the duct may be estimated. Due to variations in actual setup and duct configuration, results may have variation of ±20%.

CHAPTER XI

COMPARISON TO PREVIOUS WORK

LBNL Research

A previous study examined the effects of compression on the static pressure drop through flexible duct (Abushakra et. al, 2004)[25]. Abushakra's study tested flexible duct in a draw-through configuration with nominal compression ratios of maximum stretch, 15%, and 30%. Table 4 displays the results of the current testing and Abushakra's testing. It should be noted that the testing did not use the same compression ratios, and that the Weaver data used a blow-through configuration while Abushakra used a draw-through configuration. Due to these differences, the data cannot be directly compared; however, the two data sets show similar results for testing done by Abushakra.

	Flow	Max Stretch	15% Board Supported	30% Board Supported
	CFM	inH_2O	inH_2O	inH_2O
Abushakra et. al				
6"	100	0.109	0.458	0.984
8"	200	0.078	0.308	0.498
10"	300	0.062	0.221	0.344
Weaver et. al				
6"	100	0.081	0.561	1.052
8"	200	0.073	0.382	0.718
10"	300	0.054	0.229	0.361

Table 4. Comparison to previous research done by Abushakra et al. 2002 at LBNL

Comparison to Trane-produced Ductulator (Trane Co. 1976)

The resulting data were compared with results achieved with a duct calculator, or ductulator, typically used in the industry as displayed in Table 5. A ductulator uses input flow rate and duct size to calculate static pressure drop. The percent compression is not an input variable. Since the existing duct calculation devices have no inclusion of compression, errors in excess of five times the ductulator predicted values are possible when compared to actual installations. These ductulator results do not include ASHRAE correction factors. Due to the nature of the visually recorded ductulator values, some variation (on the order of ±5%) is expected between observations.

The error factor listed in Table 4 is a result of the measured value divided by the ductulator value. This provides a quick indication of the magnitude of the underestimation provided by the ductulator. The chosen flow rates are representative of the typical CFM found in the listed duct sizes in residential construction. The underestimation for the 4% compression cases is within a factor of ±0.6 inH_2O for all flow rates. The test results at 4% compression compare similarly to the ductulator values. Experimental results from the LBNL work concluded that flexible ducts naturally relax to about 4% compression when stretched and released. ~

	Flow	Max. Stretch	4% Joist Supported	15% Joist Supported	15% Board Supported	30% Joist Supported	30% Board Supported	45% Joist Supported	45% Board Supported
	CFM	inH_2O	inH_2O	inH_2O	inH_2O	inH_2O	inH_2O	inH_2O	inH_2O
Ductulator									
6"	100	0.155							
8"	200	0.14							
10"	300	0.095							
Measured									
6"	100	0.081	0.222	0.979	1.034	1.919	1.431	1.844	1.594
8"	200	0.073	0.146	0.382	0.405	1.428	0.767	1.204	1.204
10"	300	0.064	0.124	0.397	0.328	0.360	0.354	0.847	0.847
Error Factor									
6"	100	0.520	1.430	6.313	6.671	12.379	9.230	11.899	10.287
8"	200	0.523	1.041	2.728	2.891	10.200	5.480	8.599	8.599
10"	300	0.672	1.309	4.174	3.454	3.792	3.727	8.920	8.920

Table 5. Ductulator results comparison

CHAPTER XII

DISCUSSION

The results of this study affect residential homeowners, power providers, and equipment manufacturers alike. Designing a system to perform against the type of pressure losses observed in this testing of compressed flexible duct requires increased equipment sizing when compared to a system operating at design losses. The results of this study demonstrate that compressed flexible duct increases static pressure drop anywhere from two times to over ten times. This increase is larger in magnitude than any diverging flow fittings or register boots located in the system. This means that the installation of the ductwork is just as important as the design of the duct system, if not more so.

It should be noted that increased sag in joist supported installations from natural sag to long-term sag increases the static pressure drop in magnitude anywhere from 160% to 220%. Thus it becomes important to minimize the sag between supports in a joist-supported installation for an energy efficient design. Similarly, increases in sag rate in hung ductwork from 2" sag to 16" sag increase the static pressure losses 280% to 350%. Flexible duct in a hung configuration should then be installed to minimize sag rate between supports, as outlined in the ADC Flexible Duct Performance and Installation Standard (ADC 2003).

The results of the testing revealed other effects that impact the measured pressure drop. The change in the geometry of the airflow path within a flexible duct causes an

increase in the static pressure drop. The flow path can be altered by compressing the duct, bending the duct, or allowing the duct to sag between supports. Another parameter of interest is the increased flow length over which the air must travel induced by the helical form of the flexible duct. As the duct compression increases, this helical pattern becomes more pronounced, inducing the formation of vortices within the air stream. This means that the air encounters a longer path of travel proportional to the degree of compression, meaning more surface interactions, as it moves through the duct. This, in turn, leads to an increase in static pressure drop.

Another important observed physical effect involves the ratio-crumple region to duct diameter. The crumple region is the cross-sectional area inside the duct that shrinks as the duct is compressed. As duct compression increases, the effective inside diameter decreases, creating an accordion like effect, until the helical sections of the duct come in contact with one another. This compression creates a decrease in the cross-sectional area through which the air flows. This effect agrees with the observed higher pressure drop percentage for smaller duct sizes since this effect is more pronounced at smaller duct sizes.

CHAPTER XIII

CONCLUSIONS

Non-metallic flexible duct pressure losses, at maximum stretch, fall within 2% of rigid sheet metal losses. At compression values over 4%, non-metallic flexible duct exhibits two times to ten times increased pressure drop over sheet metal losses. Losses at higher compression values, with an internal positive duct pressure relative to the ambient, have not been previously reported. These measurements demonstrate that calculated airflows in flex-duct systems, particularly on longer duct runs, may have errors over 70% if the flexible duct compression ratio is greater than 4%.

The experimental results also demonstrate that with compression ratios exceeding 4%, the duct performance varies considerably with slight variations in the installation. The results for the as-built test protocol need to be used as a range of values that can be encountered in field installations. Static pressure losses were highly sensitive to variations in installation, with variation as much as ±20%, indicating that as-built duct installations likely experience higher static pressure losses than standard installations tested in the laboratory.

Static pressure loss data indicates that, in an as-built home, rooms served by poorly installed flexible duct will receive less airflow than designed for. Overall system airflow in a home with improperly installed flexible duct will be less than design intent, resulting in decreased total airflow and decreased cooling system performance.

REFERENCES

1. Department of Energy 2005. Residential Electricity Prices: A Consumer's Guide. http://www.eia.doe.gov/neic/brochure/electricity/electricity.html.

2. Department of Energy. 1992 Stronger Manufacturers' Energy Efficiency Standards for Residential Air Conditioners Go Into Effect Today http://74.125.95.132/search?q=cache:3Flmb5ExtwJ

3. ACCA. 1995. *Residential Duct Systems. Manual D*. Air Conditioning Contractors of America, Washington, D.C.

4. ASHRAE. 2005. *ASHRAE Handbook of Fundamentals*. American Society of Heating, Refrigerating and Air-Conditioning Engineers, Atlanta, GA.

5. Moody, L.F. 1944. "Friction Factor for Pipe Flow." *ASME Transactions* 66, pp. 671-678.

6. Trane Company. 1976. *Explanation of the Trane Air Conditioning Ductulator*. Product Explanation. Trane Co, Carrollton, TX.

7. Richards, P.E. 1988. "Air Ducts: The Uses and Abuses of Flexible Air Ducts."*Australian Refrigeration, Air Conditioning, and Heating* 42 (9) pp. 33-36.

8. Kokayko, M., J. Jolton, T. Beggs, S. Walthour, and B. Dickson, 1996. "Residential Ductwork and Plenum Box Bench Tests." *IBACOS Burt Hill Project 95006*.-13. Pittsburgh, PA.

9. Abushakra, B., D. Dickerhoff, I. Walker and M. Sherman. 2002. "Laboratory Study of Pressure Losses in Residential Air Distribution Systems." *Lawrence Berkeley National Laboratory Report LBNL-49293*, Berkeley, CA.

10. Tsal, R.J. and H.F. Behls, 1986. "Evaluation of Duct Design Methods." *ASHRAE Transactions*, 92 (1A), pp. 347-361.

11. Abushakra, B., I. S. Walker, and M. H. Sherman. 2002. "Laboratory Study of Pressure Losses in Residential Air Distribution Systems." *ACEEE Summer Study 2002*, American Council for an Energy Efficient Economy, Washington D.C.

12. ASHRAE. 1999. ASHRAE Standard 120P, Methods of Testing to Determine Flow Resistance of HVAC Air Ducts and Fittings, June 1999. American Society of Heating Refrigerating and Air-Conditioning Engineers, Atlanta, GA.

13. Tsal, R.J. 1989. "Altshul-Tsal Friction Factor Equation." *HPAC* July.

14. Altshul, A.D. and P.G. Kiselev. 1975. *Hydraulics and Aerodynamics*. Stroisdat Publishing House, Moscow, USSR.

15. Harris, A. D. 1958. "Examination of Flexible Duct." *Colliery Engineering* 35 (407), pp. 29-30.

16. Bricker, E.J. 1961. "Field Checking and Testing of Ventilation and Air Conditioning Systems." *ASHRAE Journal* May, pp. 10-72

17. Harrison, E. 1965. "Balancing Air Flow in Ventilating Duct Systems." *IHVE Journal* 33, pp. 201-226.

18. Fellows, J.R. 1939. "Power Savings through Static Pressure Regain in Air Ducts." *HPAC* 11 (4) pp. 219-222.

19. Shieh Chun-Lun, 1983. "Simplified Static-Regain Duct Design Procedure." *ASHRAE Transactions* 89 (2a), pp. 78-94.

20. Scott, K.B.1986. "Don't Ignore Duct Design for Optimized HVAC Systems." *Specifying Engineer* 62, January.

21. Tsal, R.J. and H.F. Behls. 1988. "Fallacy of the Static Regain Duct Design Method." *ASHRAE Technical Data Bulletin,* ASHRAE, Atlanta, GA

22. Ibacos 1995. "Ventilation Ducts and Registers." *IBACOS-Interim Milestone Report* , Pittsburgh, PA.

23. ADC. 2003. *Flexible Duct Performance and Installation Standards, 4th Edition*. Air Diffusion Council. Schaumburg, IL.

24. Culp, C. 2005. Private communications: Test setup flow diagram.

25. Abushakra, B., I. S. Walker, and M. H. Sherman. 2004. "Compression Effects on Pressure Loss in Flexible HVAC Ducts." *International Journal of Heating, Ventilating, Air-Conditioning and Refrigeration Research* 10 (3), pp. 275-289.

APPENDIX A
OPERATING CODE COMMENTARY

FRM Monitor

Private Sub cmdExport_Click()
Sets subroutine for command button on monitor template
cmdSaveAs.Enabled = True
Sets save command to true (when command button is pressed, it saves)
If cmdExport.Caption = "Export" Then
Begins If routine. Sets export button caption to export
cmdExport.Caption = "Stop"
Then command. Sets export button caption to stop once pressed
'Create the Excel Object
Dialog telling what is being done with next lines of code
Set xlapp = CreateObject("Excel.Application")
Activates the creation of a file using Excel
Set xlbook = xlapp.Workbooks.Open(FileName:=App.Path & "\Values.xlt")
Activates the workbook to be used with filename given
Set xlsheet = xlbook.Worksheets(1) 'Activate proper worksheet
Activates the proper worksheet to be used
xlapp.Visible = True
Makes the active Excel file visible to user
ExportFlag = True
Sets the caption on the export button to export
Else
Else command
cmdExport.Caption = "Export"
Sees if export button caption is export
ExportFlag = False
If already set to export, it doesn't change to export
End If
Ends If command
End Sub
Ends Subroutine

Private Sub cmdSave_Click()
Sets subroutine for save button on monitor template
Set xlappsave = CreateObject("Excel.Application")
Activates the Excel program
Set xlbooksave = xlappsave.Workbooks.Open(FileName:=App.Path & "\Defaults.xls")
Activates the workbook entitled defaults.xls
Set xlsheetsave = xlbooksave.Worksheets(1) 'Activate proper worksheet
Activates the proper worksheet with necessary data

With frmMonitor
Begins With statement for Monitor form

For cnt = 0 To 11
Sets counter from 0 to 11
xlsheetsave.Cells(cnt + 1, 1).Value = .Label1(cnt).Caption
Sets the value of the designated cell as the name of the sensor in line cnt
xlsheetsave.Cells(cnt + 1, 2).Value = .cboChannel(cnt).Text
Sets the value of the designated cell as the text of the channel in line cnt
xlsheetsave.Cells(cnt + 1, 3).Value = .cboMin(cnt).Text
Sets the value of the designated cell as the text of the min in line cnt
xlsheetsave.Cells(cnt + 1, 4).Value = .cboMax(cnt).Text
Sets the value of the designated cell as the text of the max in line cnt
xlsheetsave.Cells(cnt + 1, 5).Value = .txtScalar(cnt).Text
Sets the value of the designated cell as the text of the scalar in line cnt
Next cnt
Goes to next cnt and starts previous lines again until cnt = 11
End With
When cnt = 11, the With command ends
xlbooksave.Save
Saves excel workbook
xlbooksave.Close
Closes excel workbook
xlappsave.Quit
Closes excel application
End Sub
Ends subroutine

Private Sub cmdSaveAs_Click()
Sets subroutine for save as button on monitor
If cmdSaveAs.Caption = "Save As" Then
If command, checks whether the caption of button is save as
FileName = InputBox("Save file as:", "Save As")
If this is true, a file name is asked for
xlbook.SaveAs (App.Path + "\" + FileName + ".xls")
The excel workbook is saved under this file name
cmdSaveAs.Caption = "Save"
Save as button changes to say save
Else
Else command
xlbook.Save
If caption is not save as, just save workbook
End If
End If command

End Sub
End subroutine

Private Sub cmdScan_Click()
Sets subroutine for scan button on monitor
cmdExport.Enabled = True
Sets export enabled to true
StopLoopFlag = False
Sets stoploopflag to false
While Not StopLoopFlag
While command, executes loop if StopLoopFlag is false
Call DisplayReadData
Calls DisplayReadData subroutine
*Sleep (cboDelay.Text * 1000)*
Sleep command, takes number in delay box and * 1000 for time
Wend
End While loop
End Sub
End subroutine

Private Sub cmdExit_Click()
Sets subroutine for exit button on monitor
StopLoopFlag = False
Sets StopLoopFlag to false
DoEvents
Yields to processor to finish all function working at time button is pressed
Sleep 1000
Sleep command, waits 1000 milliseconds
End
Ends sleep
End Sub
Ends subroutine

Private Sub Form_Load()
Loads dubroutine
StopLoopFlag = True
Sets subroutine for layout of monitor interface
For x = 0 To 11
Begin For loop, sets values of x (line) from 0 to 11
For y = 0 To 31
Begin For loop, sets values of y from 0 to 31
frmMonitor.cboChannel(x).AddItem y
Adds value of y to drop down options for channel
Next y

Repeats previous line for each y value
Next x
Repeats second For loop for next x, loop ends after last x value
For x = 0 To 11
Begin For loop, sets values of x (line) from 0 to 11

frmMonitor.cboMin(x).AddItem
Adds value of 0 for first x in Min column drop down option
frmMonitor.cboMin(x).AddItem 0.8
Adds value of 0.8 for first x in Min column drop down option
frmMonitor.cboMin(x).AddItem 1
Adds value of 1 for first x in Min column drop down option
frmMonitor.cboMax(x).AddItem 4
Adds value of 4 for first x in Max column drop down option
frmMonitor.cboMax(x).AddItem 5
Adds value of 5 for first x in Max column drop down option
Next x
loop for next x, end loop after last x value
frmMonitor.cboDelay.AddItem 1
Adds value of 1 to Delay drop down option
frmMonitor.cboDelay.AddItem 2
Adds value of 2 to Delay drop down option
frmMonitor.cboDelay.AddItem 5
Adds value of 5 to Delay drop down option
frmMonitor.cboDelay.AddItem 10
Adds value of 10 to Delay drop down option
frmMonitor.cboDelay.AddItem 15
Adds value of 15 to Delay drop down option
frmMonitor.cboDelay.AddItem 30
Adds value of 30 to Delay drop down option
frmMonitor.cboDelay.AddItem 60
Adds value of 60 to Delay drop down option
Set xlappsave = CreateObject("Excel.Application")
Opens excel application
Set xlbooksave = xlappsave.Workbooks.Open(FileName:=App.Path &
"\Defaults.xls")
Opens workbook file Defaults.xls
Set xlsheetsave = xlbooksave.Worksheets(1) 'Activate proper worksheet
Opens proper sheet
With frmMonitor
Begin With loop, does actions stated in following loop to Monitor
For cnt = 0 To 11
Begin For loop, sets cnt values from 0 to 11
.Label1(cnt).Caption = xlsheetsave.Cells(cnt + 1, 1).Text

Sets value of the Caption in monitor to value in specified cell
.cboChannel(cnt).Text = xlsheetsave.Cells(cnt + 1, 2).Text
Sets value of the Channel in monitor to value in specified cell
.cboMin(cnt).Text = xlsheetsave.Cells(cnt + 1, 3).Text
Sets value of the Min in monitor to value in specified cell
.cboMax(cnt).Text = xlsheetsave.Cells(cnt + 1, 4).Text
value of the Max in monitor to value in specified cell
.txtScalar(cnt).Text = xlsheetsave.Cells(cnt + 1, 5).Text
Sets value of the Scalar in monitor to value in specified cell
Next cnt
Repeat for next cnt, end For loop after last cnt value
End With
End With loop
xlbooksave.Close
Closes workbook
xlappsave.Quit
Quits excel application
End Sub
Ends subroutine
Private Sub Label1_Click(Index As Integer)
Sets subroutine for clicking a label
Label1(Index).Caption = InputBox("What is the name of the sensor?", "Edit")
When a label is clicked on, caption box appears asking for name of sensor
End Sub
Ends subroutine

Mod Functions

' This subroutine is called to read in from each of the input
' devices and display the data on either the 'Monitor' window
' or the 'RunTest' window. It does not take as many readings
' as the 'ReadData' subroutine does, which means that demands
' less processing. The number of readings can be changed by
' changing the value of the 'readings' variable.

Public Sub DisplayReadData()
Sets subroutine to display the read data
Dim iStatus As Integer
Declares variable iStatus as an integer
readings = 100
Sets number of readings equal to 100
Dim dVoltage(devices + 1) As Double ' Array to hold the voltages from the NI cards

Declares array named dVoltage to hold voltage values from DAQ card

Dim total(devices + 1) As Double ' Array to sum the total of the voltage readings

Declares array named total to sum the total of the voltage readings

Dim average(devices + 1) As Double ' Array to store the averages of the readings

Declares array named average to hold average of voltage readings

' Reset the totals for calculating averages.

For cnt = 0 To devices

Begin For loop, sets value of device variable to 0

total(cnt) = 0

Sets value of total array to 0

Next cnt

Repeats for all cnt values, ends at least cnt value

' Take 100 readings from each of the analog inputs and average them

For g = 1 To readings

For loop, sets values of g from 1 to variable reading

' AI_VRead(device, channel, gain (1: 5v .5: 10v), return value)

Describes what parameters for AI_VRead are

For x = 0 To 15

Begin For loop, sets values of x from 0 to 15

With frmMonitor

Begin With loop, does following with Monitor form

If .Label1(x).Caption <> "Sensor" Then

Begin If loop, sees if caption label is Sensor

iStatus% = AI_VRead(1, .cboChannel(x), 1, dVoltage(x))

If true, then executes AI_VRead with given parameters

Else

Else command

x = x - 1

Sets x equal to x-1

Exit For

Then exit For loop

End If

Ends If loop

End With

Ends With loop

Next x

Repeat for next x, end after last x value

' Sum up the voltages

For cnt = 0 To x

Begin For loop, sets values of cnt from 0 to x

total(cnt) = total(cnt) + Abs(dVoltage(cnt))

Set value of total array to previous total array plus abs value of voltage array

Next cnt
Repeat for next cnt, end after last cnt value
DoEvents
Yields processor time to all other running programs
Next g
Repeat for next g, end after last g value
' Calculate average
For cnt = 0 To x
Applied count form 0 to X
average(cnt) = total(cnt) / readings
Specifies average of count variable
Next cnt
Proceed to next variable
With frmMonitor
Begin With loop, does following with Monitor form
' Calculate values for the readings
For cnt = 0 To x
Begin For loop, sets values of cnt from 0 to x
If frmMonitor.chkTemp(cnt).Value = Checked Then
Begin If loop, sees if Temp box on Monitor form is checked
Reading(cnt) = average(cnt)
If true, sets reading array to average array
Else
Else command (if statement false)
*Reading(cnt) = (average(cnt) - .cboMin(cnt).Text) / (.cboMax(cnt).Text – .cboMin(cnt).Text) * .txtScalar(cnt).Text*
Sets reading array to (average – Min) / (Max – Min) *Scalar
End If
End If loop
.txtVoltage(cnt) = Format(average(cnt), "0.##0")
Sets format of voltage text
.txtValue(cnt) = Format(Reading(cnt), "0.##0")
Sets format of value text
Next cnt
Repeats for next cnt value, ends after last cnt value
If ExportFlag = True Then
Begin If loop, ExportFlag is true, then
If z = 0 Then
Begin If loop, if z = 0, then
xlsheet.Cells(1, 1).Value = "Time"
Sets designated cell to “Time” text
xlsheet.Cells(1, 2).Value = "Date"
Sets designated cell to “Date” text
For y = 0 To x

Begin For loop, sets values of y from 0 to x
xlsheet.Cells(1, 3 + y).Value = .Label1(y).Caption
Sets designated cell to the caption name
Next y
Repeat for next y, end after last y value
End If
Ends If loop
z = z + 1
Sets value of z to z plus 1
xlsheet.Cells(z + 1, 1).Value = Time
Sets designated cell to "Time" text
xlsheet.Cells(z + 1, 2).Value = Date
Sets designated cell to "Date" text
For Count = 0 To x
Begin For loop, sets values of Count from 0 to x
xlsheet.Cells(z + 1, Count + 3).Value = Format(Reading(Count), "0.##0")
Sets format for designated cells
Next Count
Repeat for next Count, ends after last value of Count
End If
Ends If loop
End With
Ends While loop
End Sub
Ends subroutine

Declarations Module

Public Declare Sub Sleep Lib "kernel32" (ByVal dwmilliseconds As Long) ' Sleep Function
Declares subroutine for Sleep function
Public StopLoopFlag, ExportFlag As Boolean ' Value to stop or allow loop to start
Sets StopLoopFlag and ExportFlag to Boolean
Public Const devices = 16
Sets number of devices to 16
Public FileName As String
Sets variable FileName to a string variable
Public cnt, count As Integer
Sets variables cnt and count to an integer variable
Public x, y, z As Integer ' Used for the array of input values
Sets variables x, y, and z to an integer variable
Public VFDVolts As Double

Sets variable VFDVolts to a double variable

Public Reading(32) As Double

Sets readings as double-ended variables

Public xlapp As Excel.Application

Sets xlapp to Excel program

Public xlbook As Excel.Workbook

Sets xlbook to Excel Workbook

Public xlsheet As Excel.Worksheet

Sets slsheet to Excel worksheet

Public xlappsave As Excel.Application

Sets xlappsave to Excel program

Public xlbooksave As Excel.Workbook

Sets xlbooksave to Excel Workbook

Public xlsheetsave As Excel.Worksheet

Sets xlsheetsave to Excel Worksheet

VITA

Name:	Kevin Douglas Weaver
Address:	Department of Mechanical Engineering c/o Dr. Charles Culp Texas A&M University College Station, TX 77843-3123
Email Address:	kweaver8@gmail.com
Education:	B.S., Mechanical Engineering, Texas A&M University College Station, 2003